Calibration and Validation of a Hybrid Traffic Flow Model Based on Vehicle Trajectory Data from a Field Car-Following Experiment

Roberta Di Pace[1a], Facundo Storani[a] , Shi-Teng Zheng[b], Rui Jiang[b], Stefano de Luca [a],

[a]*Department of Civil Engineering, University of Salerno, Salerno (Italy)*

[b]*Key Laboratory of Transport Industry of Big Data Application Technologies for Comprehensive Transport, Ministry of Transport, Beijing Jiaotong University, Beijing (China)*

ABSTRACT

The paper focuses on the calibration of the hybrid multi-scale modelling approach that incorporates multiple levels of traffic flow representation. This paper refers to a model already developed in the literature, the Hybrid Cellular Automata (CA) and Cell Transmission Model (CTM). We use vehicle trajectory data collected from a car-following field experiment on a circular road track to explore the calibration of the CA model concerning various cell lengths through two distinct approaches: simulating all vehicles within the closed loop and simulating each vehicle using data obtained from its respective follower. We also evaluate different methods for the CTM calibration with respect to the CA model. The major findings are: 1) the calibrated parameters obtained using the simulated leader approach display greater regularity across different cell lengths; 2) the Constrained Squared Error [CsqE] method for macroscopic calibrations yielded promising results, showcasing the lowest sum of squared errors between fundamental diagrams.

[1] *Corresponding author: rdipace@unisa.it*

Keywords: *Cell Transmission Model; Cellular Automata; fundamental diagram; experimental data.*

1 INTRODUCTION AND MOTIVATION

We are currently witnessing a significant development and advancement in the field of connected, cooperative and automated mobility (CCAM) (Lu et al., 2023). This development is closely linked to the need for proactive traffic state estimation and forecasting (Yang et al., 2023) as well as management systems that leverage the abundance of data originating from the CCAM context (Degrande et al., 2023).

While the technological context is well-established, there is a pressing need for major advances in traffic flow modelling to effectively evaluate the impacts of connected and automated vehicles (CAVs) on transportation networks and develop appropriate traffic management and control strategies.

The primary focus of this paper is traffic flow modelling. The impact of CCAM strategies can be referred to local contexts and other more extensive contexts on a very large-scale network application. On the one hand, local-scale analyses require the development of models focusing on vehicular outflow at microscopic level, considering individual vehicles. On the other, large-scale applications, due to the expected traffic flow phenomena and the large amount of data of microscopic modelling, call for macroscopic aggregate approaches to avoid inefficiencies and excessive complexity during the implementation of CCAM strategies.

In this context, the hybrid multi-scale modelling approach (Leclercq, 2007) emerges as a viable solution. Such models incorporate multiple levels of representation rather than relying solely on a single level (e.g., macroscopic-aggregate, or microscopic-disaggregated). For instance, a multi-scale framework could employ microscopic, disaggregated modelling in areas where CCAM strategies are implemented while employing macroscopic modelling in other areas indirectly affected by the controlled infrastructure.

The hybrid approach also aligns with the coexistence of different operators responsible for controlling different infrastructures, including the primary infrastructure to be controlled and the secondary infrastructure indirectly interacting with it. From an operational standpoint, the development of CCAM mobility takes place within the framework of a real ecosystem generally managed by traffic control centres. Such centres exchange input-output data on multiple scales and involve multiple operators. Multi-scale modelling enables the discretization of the road network into several sub-networks, not only for analysis and control purposes but also for its management. This can be seen in the representation of road networks as 'federated' networks (Khan et al., 2023), where each sub-network is managed by a different operator.

Within this context, there emerges a growing need to adopt and advance hybrid multi-scale models that support CCAM ecosystems. Indeed, in the context of vehicle-to-X communication and ever faster communication protocols, specific traffic flow models are required to support suitable representation of vehicle (driver) behaviour, using the information provided by connected vehicles. Thus, it is necessary to collect and elaborate information from vehicles approaching junctions (see Zhao et al., 2021) and, at the same time, provide them with consistent information[2].

This problem is usually addressed with microscopic models as they can deal with each vehicle separately. However, they are highly detailed, require several parameters to be set, and are computationally demanding. Yet it is possible to adopt an alternative modelling approach based on a hybrid model to overcome such issues. This paper focuses on a model already developed in the literature, the H – CA&CTM (Hybrid Cellular Automata Cell Transmission Model; Storani et al., 2022) which combines a meso-

[2] That is, the traffic state that the driver will experience (Cascetta, 2006).

microscopic model (Treiber and Kesting, 2013) with a macroscopic approach. Specifically, the cellular automata model (CA; Nagel and Schreckenberg, 1992) is used as the disaggregated model, while the cell transmission model (CTM; Daganzo, 1994) serves as the aggregated macroscopic model. In a broader sense, the benefits extend across both macroscopic and microscopic levels. Macroscopic benefits include smoother traffic flow, reduced congestion and emissions, and enhancements in capacity. On a microscopic scale, benefits encompass improved lane-changing dynamics, optimized car-following behaviour, reduced reaction times, and the maintenance of safe distances between vehicles. The hybrid multi-scale modelling approach (Leclercq, 2007) can integrate various levels of representation rather than relying solely on a single level such as macroscopic-aggregate or microscopic-disaggregated models. It is important to note that while mesoscopic models, as proposed by Tordeux et al. (2014), are intermediate between micro and macroscopic approaches (the vehicles are considered individually as in a microscopic model, while their dynamics are aggregated as in a macroscopic one), they operate differently from the proposed multi-scale/hybrid model. A multi-scale framework can leverage microscopic, disaggregated modelling in areas where traffic control strategies are implemented, while employing macroscopic modelling in other areas indirectly influenced by the controlled infrastructure.

The H – CA&CTM has been preliminarily calibrated (Storani et al., 2022) but, given its complexity, a detailed discussion of the calibration procedure and the use of specific

survey data is necessary[3]. While the calibration problem is extensively discussed in the literature, particularly with reference to the microscopic model (Zhou et al., 2023), the calibration of the hybrid-multiscale model remains less explored and requires further description and discussion. The aim of the paper aims is threefold:

1. Investigate the calibration of the CA model concerning various cell lengths through two distinct approaches: simulating all vehicles together in a closed ring layout and simulating each vehicle using data obtained from its respective follower.
2. Explore different methods for the calibration of the macroscopic CTM with respect to the CA model.
3. Utilize vehicle trajectory data collected from a car-following field experiment on a circular road track for the calibration procedure. This makes possible a comprehensive comparison of methods.

The rest of paper is organized as follows: the adopted models, experimental data and calibration procedure are discussed in the Methodology section; all numerical results are shown and discussed in the Results and Discussion. The last section concludes the paper.

2 METHODOLOGY

The H – CA&CTM model combines a macroscopic Cell Transmission Model (CTM) with a meso-microscopic Cellular Automata (CA) for each link, as illustrated in Figure

[3]The proposed model was preliminary calibrated using the data collected on 400 meters of the 5 I80 highway in the USA (NGSIM I80-1, 2021), during 15 min. This section of the highway has six lanes, named from 1 to 6 from left (fastest) to right (slowest), and an incoming merging ramp, called lane 7.

1. In this model, the CA is employed to model the traffic dynamics at a detailed level near junctions, while the CTM addresses traffic flow at an aggregated level along the link.

The transition between CA and CTM, and vice versa, is facilitated through spatially extended transition zones. These zones, incorporating both sub-models, receive incoming flow from upstream, transform it, and direct it towards the downstream sub-model while preserving essential flow properties. Both CA and CTM sub-models operate discretely in both time and space. This discrete nature enables them to represent traffic flow using discrete cells, with their states evolving at each time step.

In the example link between two nodes presented in Figure 1, the initial segment utilizes the microscopic CA approach to model vehicle acceleration from the upstream junction. Subsequently, vehicles progress through the first transition, where they are transformed into a macroscopic flow modelled by the CTM sub-model. Following this, in the second transition, they undergo discretization once again using a microscopic approach, to then connect the link to the junction. This step captures detailed traffic phenomena upstream of a junction, including horizontal queue formation and discharge, congestion propagation, acceleration, speed optimization, and more. A more in-depth analysis of the entire model and information about transitions and node representations can be found in Storani et al. (2022).

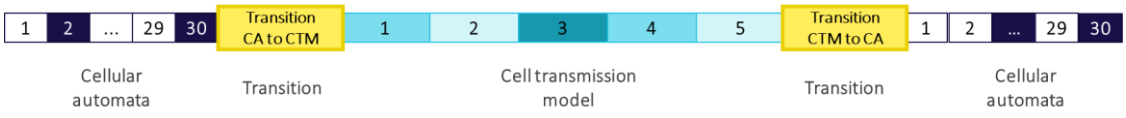

Figure 1: link modelled with H – CA&CTM, with discrete cells in each sub-model.

To maintain consistency between the CA and CTM sub-models, their parameters must be calibrated accordingly. To this end, the proposed methodology for calibration consists of three steps:

- Calibrate the microscopic model using trajectory data;
- Obtain the fundamental diagram of the calibrated microscopic model;
- Calibrate the macroscopic model based on this fundamental diagram.

2.1 Cellular Automata Model

The adopted approach was proposed by Nagel and Schreckenberg, who developed a model discrete in time and space. This model considers a single-lane road, dividing it into cells that can be “occupied” or “empty”, each with a length equal to that of a vehicle.

However, there is often criticism regarding the significance of studying traffic flow behaviour in such simplified systems. As discussed by Rickert et al. (1996), in the Nagel and Schreckenberg model, lane changing may slightly increase the capacity of the fundamental diagram, but the qualitative features remain consistent. Further analysis by Maerivoet and De Moor (2005) questions whether these basic systems can adequately capture dynamics. For instance, on many two-lane European motorways, drivers are legally required to use the right shoulder lane unless overtaking. In light traffic, slower vehicles on the right lane act as moving bottlenecks, causing faster vehicles to queue up in the left lane, resulting in density or lane inversion. In such scenarios, the stability of car-following behaviour becomes pivotal. Similarly, in heavily congested traffic, this stability determines the likelihood of a traffic breakdown. Even in multi-lane traffic, the dynamics essentially resemble those of parallel single lanes during dense congestion. Nagel and Nelson (2005) argue that assessing internal effects of a traffic flow model contributing to spontaneous breakdowns is easiest when external effects are eliminated, as in closed-loop traffic (single-lane). However, applying these models to real-life traffic networks may not always be representative, as behaviour near bottlenecks plays a more significant role.

Given these considerations, this paper focuses on further assessing the proposed hybrid traffic flow model, adopting a single lane approach. Integrating the proposed model with lane changing (LC) rules is one of the future improvements. Regarding LC rules, in recent years there has been an increased focus on studying lane-changing behaviours (Chen et al., 2004; Chowdhury et al., 1997; Jia et al., 2004, 2005; Knospe et al., 1999, 2000; Kurata and Nagatani, 2003; Lee et al., 2004; Maerivoet and De Moor, 2005; Nagai et al., 2005;Nagel et al., 1998). The basic scheme proposed by Rickert et al. (1996) essentially consist of two rules: look ahead in your own lane for obstructions and check the other lane for sufficient space. Li et al. (2006) proposed a new set of lane-changing rules, where the update step is typically divided into two sub-steps: firstly, vehicles may change lanes in parallel according to lane-changing rules, and secondly, the lanes are treated as independent single-lane Nagel and Schreckenberg models. "

In the considered single-lane model, every vehicle occupies a cell, which has an "occupied" state. In the subsequent time step, if a vehicle moves to another downstream cell, its speed is represented by an integer value (ranging from zero to a maximum value). This value signifies the number of cells the vehicle moves downstream, from position $x_i(t)$ to $x_i(t+1)$. As a consequence, the behaviour of an upstream vehicle i is influenced by a downstream vehicle $i-1$ if the gap g_i between them is smaller than the speed v_i of the upstream vehicle. The speed can be converted to a dimensional value considering the cell length and the time step. The acceleration is equal to a or 0, thereby increasing or not changing the integer value of the speed at each time step.

Additionally, the model contains a stochastic component represented by a dawdling probability. With probability p, a vehicle may either maintain its current speed (if it was accelerating) or decelerate, even if the gap is sufficient to keep accelerating. This feature enables the modelling of stop-and-go waves in congested traffic, introducing variability

into the flow-density relation as well. In more detail the parameters to be estimated are as follows:

- v_f maximum speed [m/s];
- p dawdling probability;
- a maximum acceleration [m/s^2];
- b random deceleration [m/s^2].

The model is applied by following four rules. At each time step, and for each vehicle i on the road, their speed $v_i(t)$ and position $x_i(t)$ are updated as follows:

Slowing down. Obtain the gap g_i at time t. If speed $v_i > g_i$, then slow down.

Acceleration. If speed $v_i < g_i$ gap and $v_i < v_f$, then accelerate by a.

$$v_i^*(t+1) = \min(v_i(t) + a, v_f, g_i) \quad (1)$$

Randomization (Dawdling rule). If speed $v_i > 0$, then with probability p reduce it by b.

$$v_i(t+1) = \begin{cases} \max(v_i^*(t+1) - b, 0) & with\ probability\ p \\ v_i^*(t+1) & otherwise \end{cases} \quad (2)$$

Car motion. Update the position

$$x_i(t+1) = x_i(t) + v_i(t+1) \quad (3)$$

Figure 2 illustrates an example featuring three vehicles approaching a red light in a CA-modelled link, with a length of 7 cells during 5-time steps. The cell length is set to 5 meters, a time step of 1 second, and acceleration and random deceleration set to 1. For each vehicle i at each time step t, it presents their speed $v_i(t)$, gap $g_i(t)$, and position $x_i(t)$. It is noteworthy that vehicle 3 in time step 4 activated the dawdling rule, so it did not accelerate.

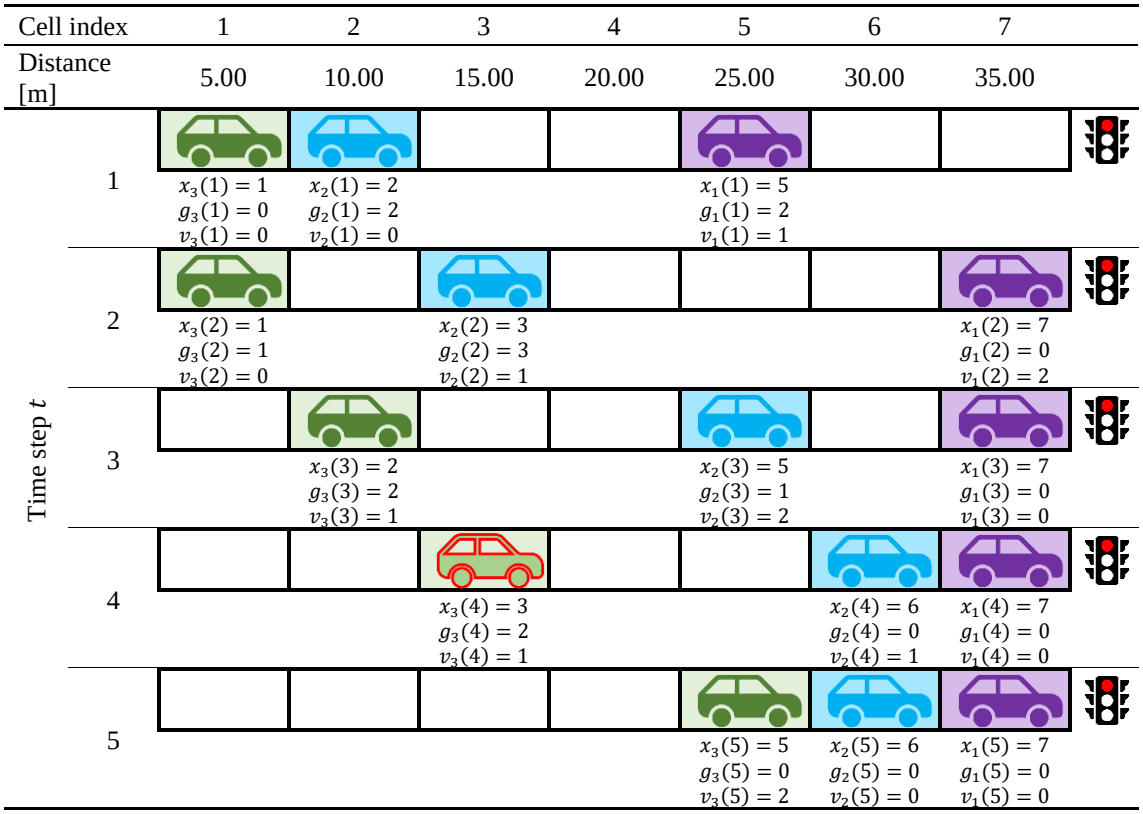

Figure 2: an example of three vehicles approaching a red light in a link modelled with CA, with 7 cells during 5 seconds.

2.2 Cell Transmission Model

The Cell Transmission Model (CTM; Daganzo 1995) is a macroscopic traffic flow model widely used model for simulating traffic flow. The CTM divides the roadway into discrete cells i, where each cell represents a segment of the road with uniform characteristics such as capacity, speed, and density. These cells are interconnected, and traffic flow is governed by a set of fundamental traffic equations that determine the rate of vehicles entering, exiting, and traveling within each cell. The CTM is a first-order discrete Godunov approximation of the kinematic wave equation, a continuous model of traffic flow, resulting in a linear macroscopic fundamental diagram.

The parameters of the model include:

- k_j jam density [veh/m];
- Q_i maximum flow rate in cell i [veh/s];

- V_f free flow speed [m/s];
- ω shock wave speed in congested traffic [m/s];
- Δx cell length [m];
- Δt time step [s];

While the main variables of the model are:

- k_i density in cell i [veh/m];
- Y_i flow exiting the boundary of cell i [veh/s].

The density of each cell is updated at each time step as a function of flows at the cell boundaries, following the conservation equation, as in the following:

$$k_i(t+1) = k_i(t) + [Y_{i-1}(t) - Y_i(t)] \cdot \Delta t/\Delta x \quad (4)$$

The maximum flow that can be *sent* (that is the *demand*) by cell i (upstream of the boundary) is given by:

$$D_i(t) = \min(Q_i, V_f \cdot k_i) \quad (5)$$

The maximum flow that can be *received* (that is the *supply*) by the downstream cell $i + 1$ is given by:

$$S_{i+1}(t) = \min\left(Q_{i+1}, \omega \cdot (k_j - k_{i+1})\right) \quad (6)$$

These linear flow-density relationships are displayed in Figure 3. As each cell has a maximum density (k_j), the incoming flow is constrained not only by the maximum value Q_{i+1}, but also by the difference between the maximum density and the current density ($k_j - k_i + 1$). This captures the spillback phenomena and models the effects of horizontal queuing.

In line with the Godunov scheme, the flow $Y_i(t)$ can be rewritten based on the demand (sending)-supply (receiving) rule of the cell transmission model as:

$$Y_i(t) = \min\left(D_i(t), S_{i+1}(t)\right) \tag{7}$$

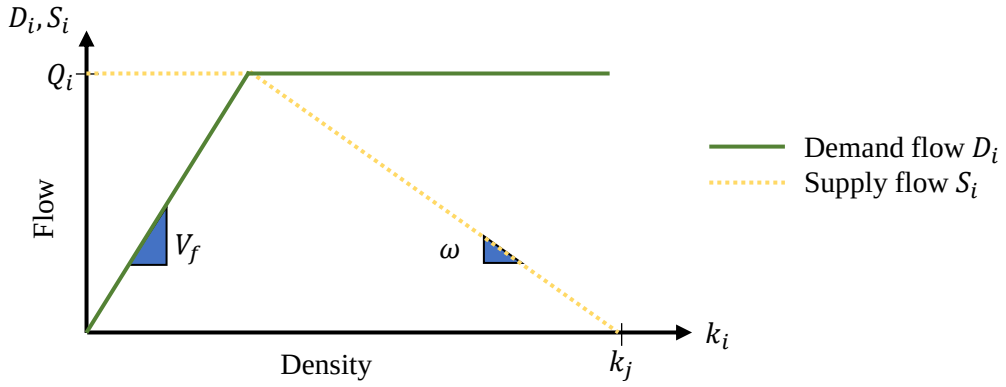

Figure 3: Linear fundamental diagram of the CTM

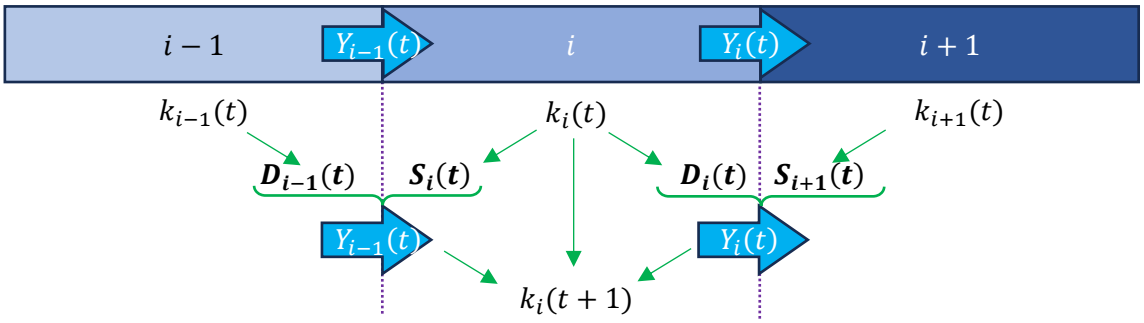

Figure 4: sequence to update the macroscopic vehicular density of each cell i at every time step t with the Cell Transmission Model, following equations (4) to (7)

The CTM has several advantages compared to other traffic flow models. Its implementation is relatively simple, and it can be used to simulate a wide variety of traffic scenarios. The CTM is also relatively efficient, which makes it suitable for simulating large transportation networks, providing insights into traffic patterns, bottlenecks, congestion, and the impact of various traffic control strategies. However, the CTM also has some limitations. It does not explicitly model the behaviour of individual vehicles, and it can be inaccurate in some situations, such as when traffic is highly congested.

2.3 Experimental data

For this study, we utilized vehicle trajectory data obtained from a field car-following experiment conducted on a closed circular road track. The experiment took place on November 9, 2019, at the test field affiliated with the Research Institute of Highway, Ministry of Transport, China. High-precision GPS devices were installed on all cars, recording vehicle trajectory data including locations and velocities at a frequency of 10 Hz. Throughout the experimental runs, the drivers followed the instruction to "Drive as if you were on a rush hour expressway. Follow the vehicle ahead closely, whenever safety permits". Further details can be found in Zheng et al. (2021).

The experiment involved 40 cars/drivers, classified into eight groups (A to H). The order of cars/drivers within each group remained fixed, but the number of groups and their order varied between runs. The specific settings of the experiment runs are presented in Table 1. As the circular track has a circumference of 812 meters, the experimental runs with 40, 35, and 30 cars corresponded to vehicle densities of 49.3, 43.1, and 37.0 vehicles per kilometre, respectively.

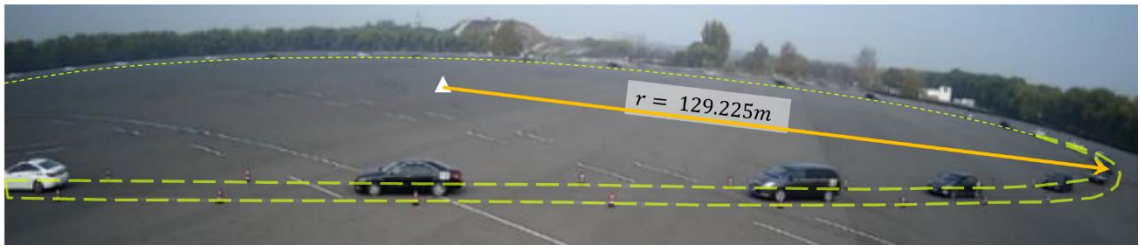

Figure 5: snapshot of a part of the experimental track, retrieved from Zheng et al. (2021), with the radius of the circumference.

2.4 Calibration procedure of the microscopic model

The trajectories obtained from the experiment have coordinates (X, Y). Given the radius of the circumference, the reference system is transformed to consider the position of each vehicle on the circumference $[0\,m\ -2\cdot\pi\cdot 125.255\,m]$, increasing in the direction of vehicle movement. A filter was applied to ensure that the vehicle positions are always increasing, avoiding negative displacements (except when the reference system restarts). For each run, an initial and final time step is defined in which all vehicles are in motion. Due to the stochastic nature of the CA model resulting from the application of the dawdling rule, a multiple simulation approach is employed by simulating each trajectory several times.

Table 1 Experiment details and summary of the data extracted for the calibration procedure

Experiment			Data for calibration					
Run ID	Number of vehicles [veh]	Net Duration [s]	Net number of vehicles [veh]	Start time [s]	End time [s]	Duration [s]	Vehicles duration [veh h]	Average total distance [km]
1	40	1680	40	165	1550	1385	15.39	13.30
2	35	1420	35	260	1240	980	9.53	11.65
3	30	690	30	85	520	435	3.63	6.34
4*	40	1680	40	150	230	80	0.89	0.71
5*	35	1420	33*	330	1250	920	8.43	9.81
6	40	1680	40	300	1510	1210	13.44	11.04
4*	40	1680	38*	250	1570	1320	13.93	12.51

** Run 4 is divided into two intervals, due to an Electronic Stability Program (ESP) fault of a vehicle during the experiment, while run 5 has missing data on one of the vehicles, so the affected vehicles and its followers were omitted on the calibration procedure (Zheng, et al., 2021).*

2.4.1 Measured Leader – Simulated Follower interaction approach

For each run and each vehicle, the measured position of the vehicle and that of its leader obtained from the experiment are extracted. The trajectory of the vehicle is then simulated 100 times[4] using the cellular automata model, applying the multiple runs method. In this

[4] The repeated simulations approach has been discussed in several studies (Laval et al., 2014; Tian et al., 2016); as suggested by Tian et al., (2021). In this paper, initially 200 simulations were considered. However, after a preliminary

case, each CA-simulated vehicle i interacts with the measured position of its respective leader from the experiment.

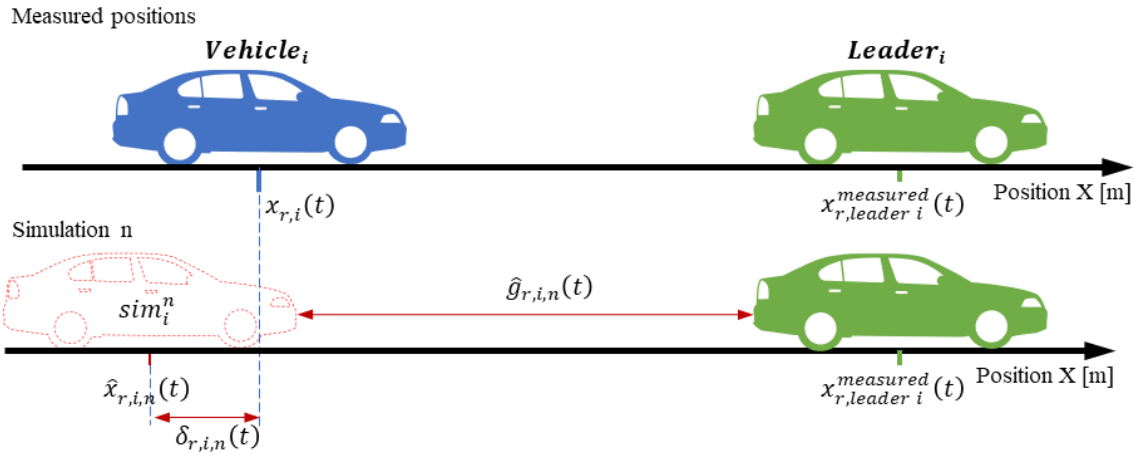

Figure 6 Measured Leader - Simulated Follower interaction approach

Let:

t be the time step,

i be the index of the vehicles,

r be the index of each experimental run,

n be the index of each simulation run,

$x_{r,i}(t)$ be the observed (measured) position of vehicle i in run r at time step t,

$\hat{x}_{r,i,n}(t)$ be the n-simulated position of vehicle i in run r at time step t,

$\hat{g}_{r,i,n}(t)$ be the n-simulated gap between vehicle i in run r at time step t and its leader,

T_r the total number of time steps in experimental run r,

V_r the total number of vehicles in experimental run r,

R the total number of experimental runs r,

N the total number of simulations runs n

---

calibration of the model, it was observed that the results stabilized after 100 simulations. Therefore, this number was adopted as the final setting.

The sum of the squared error of the position of vehicle i in run r for simulation n is:

$$\delta_{r,i,n}^2 = \sum_{t=1}^{T_r} \left(\hat{x}_{r,i,n}(t) - x_{r,i}(t) \right)^2 \tag{8}$$

Considering all the runs of the experiment and all the vehicles, the Root Mean Squared Error (RMSE) for each simulation n can be calculated as:

$$RMSE_n = \sqrt{\frac{\sum_{r=1}^{R} \sum_{i=1}^{V_r} \left(\delta_{r,i,n}^2 \right)}{\sum_{r=1}^{R} (T_r \cdot V_r)}} \tag{9}$$

During the parameter calibration of the cellular automata model, the objective is to minimize the mean RMSE across all simulations, which can be expressed as:

$$z = \min \left(\underset{n}{\text{mean}}\, RMSE_n \right) \tag{10}$$

where N is equal to 100 simulations.

Considering the mean difference across N simulations between each simulated vehicle and its measured position, it is possible to obtain an error matrix with elements $\delta_{r,i}$ as:

$$\delta_{r,i} = \underset{n}{\text{mean}}\left(\delta_{r,i,n} \right) = \underset{n}{\text{mean}} \left(\frac{\sum_{t=1}^{T_r} \left(\hat{x}_{r,i,n}(t) - x_{r,i}(t) \right)}{T_r} \right) \tag{11}$$

Additionally, it is possible to calculate the minimum RMSE for each vehicle across N simulations, resulting in an RMSE matrix with elements $RMSE_{r,i}$ expressed as:

$$RMSE_{r,i} = \sqrt{\frac{\min\limits_{n} \left(\delta_{r,i,n}^2 \right)}{T_r}} \tag{12}$$

2.4.2 Simulated Leader - Simulated Follower interaction approach

In this procedure, each experimental run is simulated entirely using the cellular automata model. Leader-follower interactions occur between simulated vehicles, with their starting

positions and speeds set to the measured values at the selected start time of each run. It is important to consider the total distance travelled by each *measured* and *simulated* vehicle at each time step, rather than solely their position within the closed ring layout, to evaluate the tracking of the vehicles' general trajectory over time and determine whether the simulation accurately reproduces the distance covered by the actual vehicle at each time step.

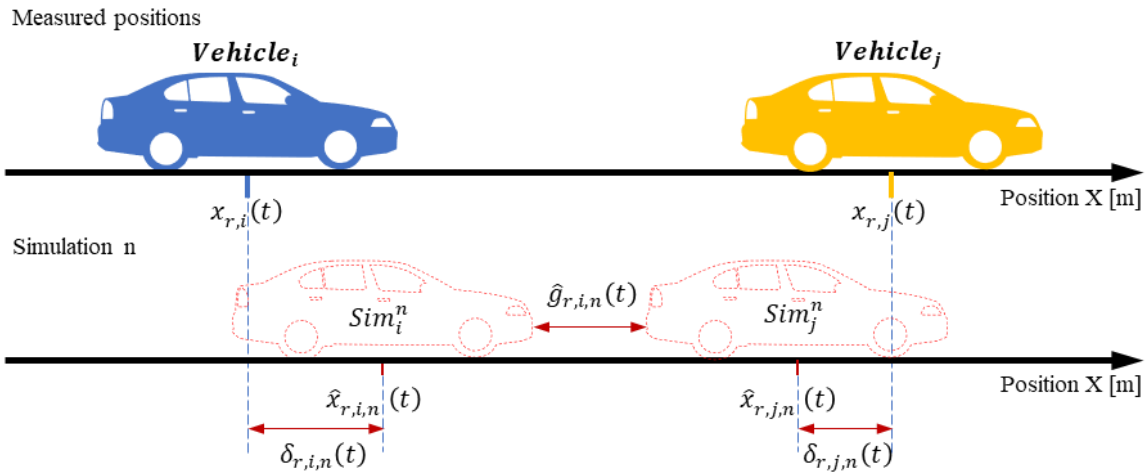

Figure 7 Simulated Leader - Simulated Follower interaction approach.

To this end, let

L be the perimeter of the circumference;

$\eta_{r,i}(t)$ be the number of times the measured vehicle i of run r passed through the starting point of the reference system of the circumference at time step t;

$\hat{\eta}_{r,i,n}(t)$ be the number of times the n-simulated vehicle i of run r passed through the starting point of the reference system of the circumference at time step t;

equation (8) is modified and rewritten as

$$\delta_{r,i,n}^2 = \sum_{t=1}^{T_r} \left(\left(\hat{x}_{r,i,n}(t) + \left(\hat{\eta}_{r,i,n}(t) \cdot L \right) \right) - \left(x_{r,i}(t) + \left(\eta_{r,i}(t) \cdot L \right) \right) \right)^2 \qquad (13)$$

The same equations (9)-(12) then apply.

2.5 Optimization procedure

Differential Evolution is applied to search the optimal values of the model parameters that minimize the set objective, subject to some constraints, consistent with engineering principles. The optimization process involves generating a random population of candidate solutions, vectors of parameter values, and iteratively improving them using the DE operators, such as mutation, crossover, and selection, until a stopping criterion is met, such as convergence or a maximum number of iterations.

2.6 Calculation of the fundamental diagrams

To derive the fundamental diagram of the microscopic model, a circular road with a circumference of 5000 meters is simulated to understand the variation in traffic flow and speed with vehicle density. The simulation is executed for various vehicle densities, ranging from 1 to 1000 vehicles, with each simulation repeated 100 times to account for the stochastic nature of the model.

In each simulation, the vehicles are initially evenly distributed on the circular road. The simulation runs for 4600 seconds, with the first 1000 seconds used as a warm-up period during which no data are collected. Data on vehicle flow and speed are collected at 10 sections located every 500 meters on the circular road, at intervals of 15 minutes. The average flow and speed are then calculated for each vehicle density value and for each of the 100 simulations, allowing for an analysis of the variation of these indicators within and between simulations. The aggregated characteristics of the resulting fundamental diagram serve as input for the Cell Transmission Model (CTM).

2.7 Calibration of the macroscopic model

The macroscopic model is calibrated based on the fundamental diagram of the microscopic results. The parameters to be estimated are the free flow speed v_f, the wave

speed ω, and the outflow capacity Q. With these parameters, it is possible to calculate the following characteristics and indicators:

The critical densities k_{c1} and k_{c2} are calculated as:

$$k_{c1} = Q/V_f \tag{14}$$

$$k_{c2} = Q/\omega + k_j \tag{15}$$

The absolute difference between the CTM and CA flows are calculated as:

$$\left|\delta_{flow}\right| = abs(q_k^{CA} - q_k^{CTM}) \tag{16}$$

The sum of the squared error is calculated as:

$$\delta_{flow}^2 = \sum\nolimits_k (q_k^{CA} - q_k^{CTM})^2 \tag{17}$$

The RMSE of the flow-density as:

$$RMSE_{flow} = \sqrt{\frac{\sum_k (q_k^{CA} - q_k^{CTM})^2}{n}} \tag{18}$$

To obtain the required parameters, three calibration methods are considered:

1. Fundamental Diagram based – [FD]
2. Squared error based - [SqE]
3. Constrained Squared error based - [CSqE]

2.7.1 Fundamental Diagram based – [FD]

The free flow speed V_f, the maximum outflow capacity Q, and the shockwave speed ω are obtained directly from the results of the fundamental diagrams of the CA models, as

$$V_f = \max(v_k^{CA}) \tag{19}$$

$$Q = \max(q_k^{CA}) \tag{20}$$

$$\omega = \min\left(-\frac{q_k^{CA}}{k_j - k}\right) \tag{21}$$

2.7.2 Squared error based - [SqE]

The maximum outflow capacity Q is obtained directly from the results of the fundamental diagrams of the CA models as

$$Q = \max(q_k^{CA}) \tag{22}$$

The free flow speed V_f and the shockwave speed ω are obtained by minimizing the sum of the squared error, with the objective of the optimization as:

$$z = \min \delta_{flow}^2 = \min \sum\nolimits_k (q_k^{CA} - q_k^{CTM})^2 \tag{23}$$

In which:

$$q_k^{CTM} = \begin{cases} V_f \cdot k & if: k < k_{c1} \\ Q & if: k_{c1} \le k \le k_{c2} \\ \omega \cdot (k - k_j) & if: k_{c2} < k < k_j \end{cases} \tag{24}$$

With V_f and ω optimization variables, subject to the following constraints:

$$10[km/h] <= V_f <= 80[km/h] \tag{25}$$

$$-20[km/h] <= \omega <= -1[km/h] \tag{26}$$

$$k_{c1} \le k_{c2} \tag{27}$$

2.7.3 Constrained Squared error based - [CSqE]

The free flow speed V_f, the shockwave speed ω, and the maximum outflow capacity Q are all obtained by minimizing the sum of the squared error, with the same optimization objective, flow equation, and constraints of [SqE] method, with the added constraint on Q as:

$$1600[veh/h] <= Q <= 2000[veh/h] \tag{28}$$

3 RESULTS

3.1 MICROSCOPIC CALIBRATION

The parameters of the cellular automata model were calibrated simultaneously with a fixed simulation time step duration of 1 second. In the considered CA model, the reaction time is implicitly equal to the duration of the time step, as it is not an explicit parameter of the model.

The vehicle length considered is 5 meters, resulting in a jam density of 200 vehicles per km. The discrete number of cells that each vehicle occupies is a multiple of the cell length, which was pre-set for better comparison and reproducibility of the results, creating several scenarios (A-E) with cell lengths equal to 5 m., 2.5 m.,1 m., 0.1 m., and 0.01 m. respectively, summarized in Table 2. The maximum speed was limited to 35 m/s, the dawdling probability to 0.9, the acceleration and the random deceleration to 5 m/s^2. The minimum increments of speed, acceleration and decelerations are given by the cell length of each scenario and the time step.

Table 2: Calibration scenarios (A-E) set with fixed cell lengths

Scenario	Calibration scenarios	Cell length [m]	Number of cells occupied by a vehicle	Cell index for a vehicle in x = 10m
A		5.00	1	2
B	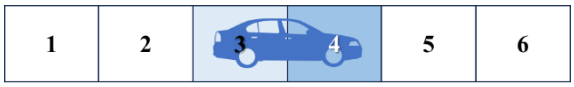	2.50	2	4
C		1.00	5	10
D	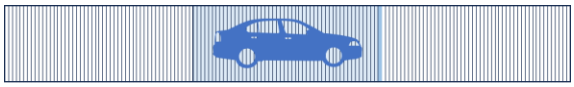	0.10	50	100
E	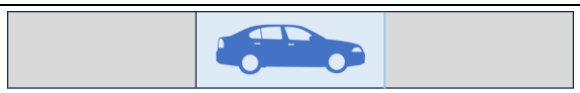	0.01	500	1000

The numerical results for the measured leader and simulated leader approaches are presented in Table 3 and Table 4, considering each cell length scenario. The

corresponding fundamental diagrams of average flow-density are illustrated in Figure 8 and Figure 9. Additional figures for each calibration result can be found in Di Pace et al. (2023), containing the standard deviation of the flow for each density in each simulation and the average speed-density diagram.

3.1.1 Measured Leader – Simulated Follower interaction

The calibration results obtained for the "measured leader" approach (Table 3) show that the Scenario A, with the longest cell and therefore the highest acceleration and random deceleration, has the highest maximum speed and the lowest dawdling probability. Scenarios D and E provide very similar results, followed by Scenario C with a slightly lower dawdling probability but higher acceleration and maximum speed due to its cell length. Scenario B has the smallest acceleration and random deceleration among all scenarios, but it has a slightly higher maximum speed than Scenarios C to E. The resulting dawdling probability falls between that of Scenarios C and D/E.

Table 3 Calibration results for the interaction between Measured Leader – Simulated Follower

Results	**1-A**	**1-B**	**1-C**	**1-D**	**1-E**
Delta time [s]	1	1	1	1	1
Cell length [m]	5	2.5	1	0.1	0.01
Maximum Speed [m/s]	20	17.5	17	16.9	16.92
Dawdling probability	0.1864	0.2687	0.2544	0.2716	0.2716
Acceleration [m/s^2]	5	2.5	3	2.7	2.69
Random deceleration [m/s^2]	5	2.5	3	2.7	2.69
Average RMSE matrix [m]	9.15	8.31	8.18	8.14	8.13
Average error matrix [m]	3.64	2.98	2.73	2.76	2.78
Objective function* $z = \min\left(\underset{n}{\text{mean}}\, RMSE_n\right)$	10.03	9.21	9.08	9.05	9.05

**This is the objective function used in the calibration procedure*

The fundamental diagram of result 1-A (see Figure 8 a) has a smooth transition between the uncongested and congested state. The standard deviation of the mean vehicle flow

between each simulation reaches a maximum close to 10 at the transition densities, while the standard deviation of the mean flow in each simulation gives its highest variability between 20 and 80 vehicles per hour in the congested segment.

The fundamental diagram of result 1-B (see Figure 8 b) has an abrupt transition between the uncongested and the congested state. Such a phenomenon is observed in the speed-density diagram given by an immediate drop of the graph from speed to free flow. The standard deviation of the mean vehicle flow between each simulation reaches a maximum of about 50 vehicles per hour at the transition densities, which is then rapidly reduced to 20 vehicles per hour and continues to fall as the density increases.

The fundamental diagram of result 1-C (see Figure 8 c) has a steep transition between the uncongested and the congested state, but less pronounced than result 1-B. Such a phenomenon is observed in the speed-density diagram given by a smoother drop of the graph from the free flow speed. The standard deviation of the average vehicle flow between each simulation reaches a maximum of about 20 vehicles per hour at transition densities, which is then rapidly reduced to 15 vehicles per hour and continues to fall as the density increases.

The fundamental diagram of result 1-D (see Figure 8 d) has a steep transition between the uncongested and the congested state, more pronounced than 1-C but less than result 1-B. Such a phenomenon is observed in the speed-density diagram given by a smoother drop of the graph from the free flow speed. The standard deviation of the average vehicle flow between each simulation reaches a maximum of about 30 vehicles per hour at transition densities, which is then rapidly reduced to 15 vehicles per hour and continues to fall as the density increases.

The fundamental diagram of result 1-E (see Figure 8 e) has similar characteristics as 1-D since its parameters are very similar. The standard deviation of the average vehicle flow

between each simulation reaches a maximum of about 30 vehicles per hour at transition densities, which is then rapidly reduced to 15 vehicles per hour and continues to fall as the density increases.

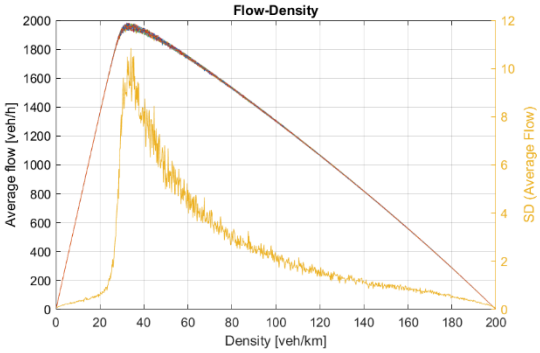

a) Fundamental Diagram Result 1-A

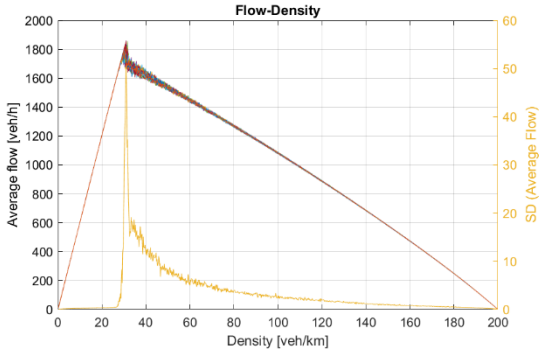

b) Fundamental Diagram Result 1-B

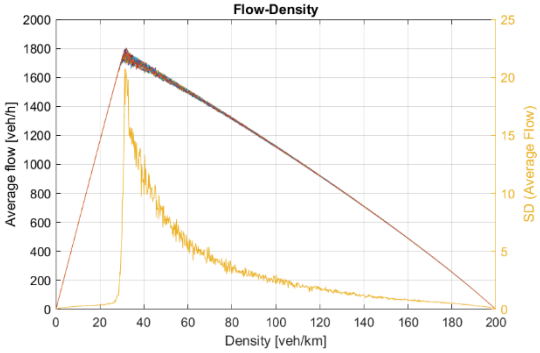

c) Fundamental Diagram Result 1-C

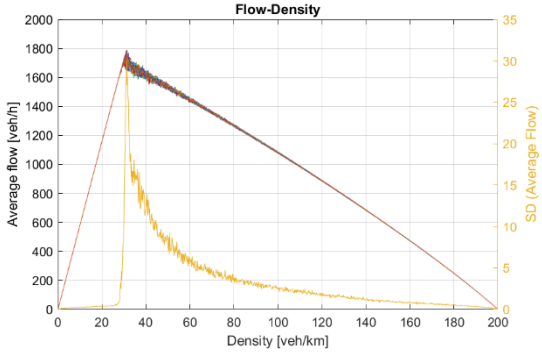

d) Fundamental Diagram Result 1-D

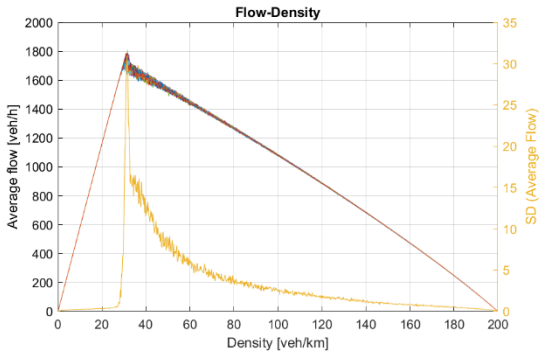

e) Fundamental Diagram Result 1-E

Figure 8 Fundamental Diagrams of approach 1: Measured Leader – Simulated Follower interaction

3.1.2 Simulated Leader - Simulated Follower interaction

The calibration results obtained for the "simulated leader" approach (Table 4) show that Scenario A, with the longest cell and therefore highest acceleration and random deceleration, has the highest maximum speed and a slightly higher dawdling probability. Scenarios B to E are very similar in terms of their maximum speed and dawdling probability. The final value of the objective function decreases slightly from C to D as the cell length decreases but not to the same order of magnitude as the cell length.

Table 4 Calibration results for the interaction between Simulated Leader (SL) – Simulated Follower (SF)

Results	**2-A**	**2-B**	**2-C**	**2-D**	**2-E**
Delta time [s]	1	1	1	1	1
Cell length [m]	5	2.5	1	0.1	0.01
Maximum Speed [m/s]	20	15	15	15.1	15.28
Dawdling probability	0.2443	0.2300	0.2312	0.2314	0.2296
Acceleration [m/s^2]	5	2.5	2	1.9	1.98
Random deceleration [m/s^2]	5	2.5	2	1.9	1.98
Average RMSE matrix [m]	246.22	233.72	226.16	223.90	229.98
Average error matrix [m]	-11.09	49.52	31.63	32.05	41.67
Objective function* $z = \min\left(\underset{n}{\text{mean}}\, RMSE_n\right)$	292.39	293.22	290.66	288.47	288.27

**This is the objective function used in the calibration procedure*

The fundamental diagram of result 2-A (see Figure 9 a) has a smooth transition between the uncongested and congested state, which can also be observed in the speed-density diagram. The standard deviation of the mean vehicle flow between each simulation reaches a maximum close to 10 at the transition densities.

The fundamental diagram of result 2-B (see Figure 9 b) has a marked transition between the uncongested and the congested state. Such phenomenon is observed in the speed-density diagram given by a pronounced drop of the graph from the free flow speed. The standard deviation of the average vehicle flow between each simulation reaches a

maximum close to 25 vehicles per hour at transition densities, which is then rapidly reduced to 15 vehicles per hour and continues to fall as the density increases.

The fundamental diagram of result 2-C (see Figure 9 c) has an abrupt transition between the uncongested and the congested state compared with result 2-B. The standard deviation of the average vehicle flow between each simulation reaches a maximum close to 55 vehicles per hour at transition densities, which is then rapidly reduced to 15 vehicles per hour and continues to fall as the density increases.

The fundamental diagram of result 2-D (see Figure 9 d) has an even steeper transition between the uncongested and the congested state compared with result 2-C. The standard deviation of the average vehicle flow between each simulation reaches a maximum close to 70 vehicles per hour at transition densities, which is then rapidly reduced to 15 vehicles per hour and continues to fall as the density increases.

The fundamental diagram of result 2-E (see Figure 9 e) has a similar trend compared to 2-D. The standard deviation of the average vehicle flow between each simulation reaches a maximum close to 60 vehicles per hour at transition densities, which is then rapidly reduced to 15 vehicles per hour and continues to fall as the density increases.

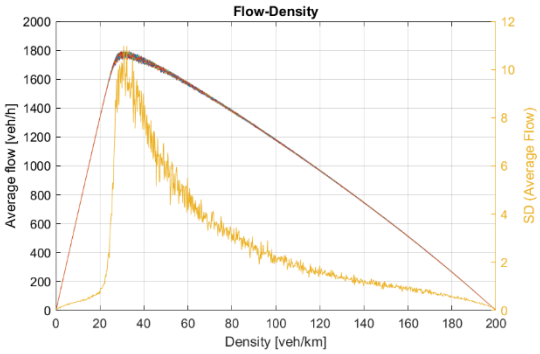

a) Fundamental Diagram Result 2-A

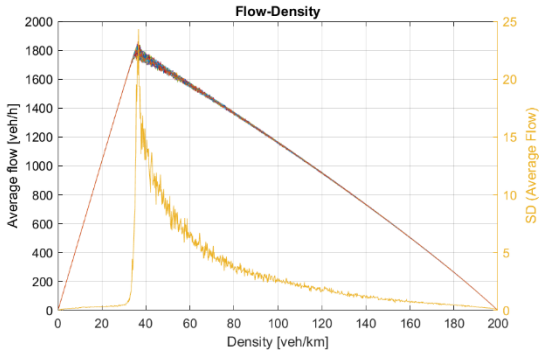

b) Fundamental Diagram Result 2-B

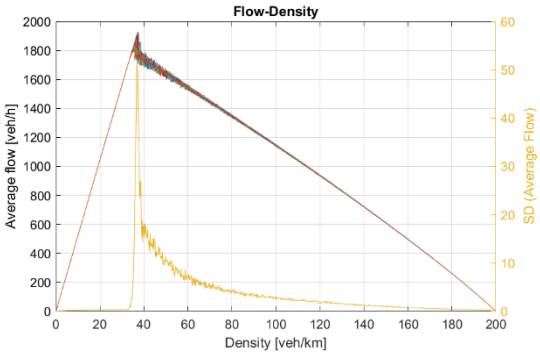

c) Fundamental Diagram Result 2-C

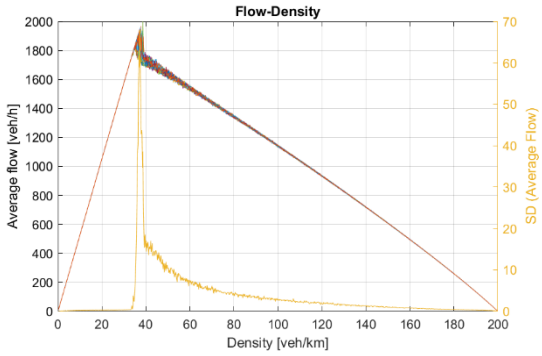

d) Fundamental Diagram Result 2-D

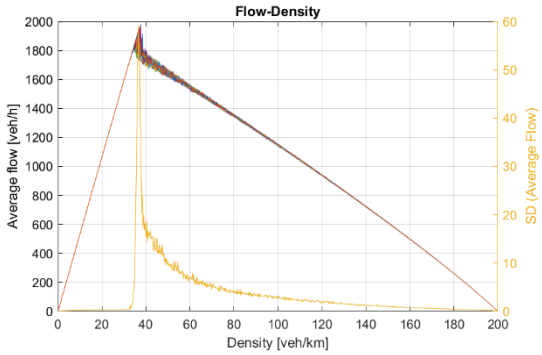

e) Fundamental Diagram Result 2-E

Figure 9 Fundamental Diagrams of approach 2: Simulated Leader – Simulated Follower interaction

3.1.3 Cross analysis

To evaluate the results of one approach applied to the other, two indicators were considered, calculated across 500 simulations[5] for each scenario and approach:

- the minimum mean RMSE across all the simulations (in Table 6), which is the same objective function of the calibration procedure described by Equation (10), to compare with the results obtained in Table 3 and Table 4;
- the RMSE obtained with the best trajectory simulated for each vehicle (in Table 7), that is, using the trajectory with the minimum sum of the square error for each vehicle in each run across the 500 simulations, calculated as:

$$RMSE_{\min \delta_{r,i,n}^2} = \sqrt{\frac{\sum_{r=1}^{R} \sum_{i=1}^{V_r} \min_{n} \left(\delta_{r,i,n}^2\right)}{\sum_{r=1}^{R} (T_r \cdot V_r)}} \tag{29}$$

Each indicator is initially calculated using the parameters calibrated for Measured Leader approach 1 (see Table 3). These calibrated parameters are then applied to the same Measured Leader approach 1 to establish a reference value. Next, the parameters calibrated for the Simulated Leader approach 2 (refer to Table 4) are applied to the Measured Leader approach 1 to determine the cross-validation value ($2 \rightarrow 1$). The percentage difference compared to the reference value is calculated for each cell-length scenario.

Similarly, the same process is followed to find the cross-validation value ($1 \rightarrow 2$) by applying the calibrated parameters of Measured Leader approach 1 to the Simulated

[5] For this analysis, the number of simulations has been increased, since the parameters are fixed and the second indicator considered depends on the single best trajectory found for each vehicle, instead of the aggregated result of the mean RMSE value used during the calibration process.

Leader approach 2. In this case, the results obtained from the Simulated Leader approach 2 are used as the reference values. A summary of the procedure is shown in Table 5. Table 6 and Table 7 display the indicator values for different cell length scenarios. The smallest value for each indicator across all scenarios is highlighted in bold, and the bold percentage difference reflects the smallest variation within each scenario.

Table 5: Summary of the procedure of the cross-analysis

Indicator	Calibrated on	Applied to	Description	ID Cross Analysis
$z = \min\left(\underset{n}{\text{mean}}\, RMSE_n\right)$	1 - ML	1 - ML	Result 1 → 1 - Measured L.	1 → 1
	2 - SL	1 - ML	Cross validation 2 → 1	2 → 1
	2 - SL	2 - SL	Result 2 → 2 - Simulated L.	2 → 2
	1 - ML	2 - SL	Cross validation 1 → 2	1 → 2
$RMSE_{\min \delta^2_{r,i,n}}$	1 - ML	1 - ML	Result 1 → 1 - Measured L.	1 → 1
	2 - SL	1 - ML	Cross validation 2 → 1	2 → 1
	2 - SL	2 - SL	Result 2 → 2 - Simulated L.	2 → 2
	1 - ML	2 - SL	Cross validation 1 → 2	1 → 2

**ML=Measured Leader approach; SL=Simulated Leader approach;*

Table 6: Cross analysis results of the minimum mean RMSE of the position [m] across 500 simulations

ID Cross Analysis	CELL LENGTH SCENARIOS				
	A	**B**	**C**	**D**	**E**
	5.00 m	2.50 m	1.00 m	0.10 m	0.01 m
1 → 1	10.02	9.20	9.08	9.05	9.04
2 → 1	**10.09(+0.7%)**	24.88(+170.3%)	20.98(+131.0%)	17.53(+93.8%)	13.78**(+52.3%)**
2 → 2	294.89	299.25	295.10	293.83	287.34
1 → 2	798.29(+170.7%)	531.12**(+77.5%)**	**370.91(+25.7%)**	541.40**(+84.3%)**	541.16(+88.3%)

Table 7: Cross analysis results of the RMSE of the position [m] with the best trajectory across 500 simulations

ID Cross Analysis	CELL LENGTH SCENARIOS				
	A	**B**	**C**	**D**	**E**
	5.00 m	2.50 m	1.00 m	0.10 m	0.01 m
1 → 1	9.34	8.42	8.37	8.32	8.32
2 → 1	**9.19 (-1.6%)**	18.47**(+119.4%)**	16.13 **(+92.7%)**	13.42 **(+61.3%)**	10.54 **(+26.7%)**
2 → 2	106.66	71.11	72.56	73.03	74.46
1 → 2	559.08(+424.2%)	297.16(+317.9%)	**170.82**(+135.4%)	289.35(+296.2%)	284.63(+282.3%)

Analysing the results of $RMSE_{\min \delta_{r,i,n}^2}$ in Table 7, the percentual differences in the cross validations are lower in all the cell length scenarios when the simulated leader approach 2 is applied to a measured leader approach 1 (i.e., 2 → 1) instead of the opposite 1 → 2, which means that the simulated leader parameters 2 have lower errors on the leader-follower interaction 1 than the measured leader 1 on the global behaviour of vehicles 2 described by their trajectory. This is not the case if it is analysed in terms of $\min\left(\underset{n}{\text{mean}}\, RMSE_n\right)$ of Table 6, which was the objective function of the calibration process, since the cross validation 2 → 1 has lower percentual difference only in cell length scenarios A and E.

In this analysis, the model parameters are fixed and constant to all vehicles in all the runs; the measured trajectory of the vehicles in the experiments are observations of a complex phenomenon driven not only by physical and mechanical limitations, but also by the behaviour of the driver. As a result, the trajectory described by a driver/vehicle may always be different even under the same context. This context may be described by aggregated characteristics, such as the vehicular density, average speed, and the average flow. The dawdling rule in the cellular automata model adds a stochastic component to the trajectories of the vehicles, even under the same context. For this reason, in this analysis it is better to compare the "best trajectory" described by the CA of each vehicle, which means analyse the results of Table 7 containing $RMSE_{\min \delta_{r,i,n}^2}$.

3.2 MACROSCOPIC CALIBRATION

In this section the results about the macroscopic calibration are shown; in more detailed the CTM calibration has been done through three methods as preliminarily described in Section 2.7. For each approach results are summarized in Table 8 and the flow - density diagrams of the macroscopic model are displayed from Figure 10 to Figure 13 .

Table 8: Macroscopic parameters obtained with each optimization method for the Measured Leader (ML) and Simulated Leader (SL) approaches

Optimization method	Calibration Approach	Model Parameters*	SCENARIOS				
			A 5.00 m	**B** 2.50 m	**C** 1.00 m	**D** 0.10 m	**E** 0.01 m
FD	1 - ML	V_f [km/h] FORMULA	69.00	61.00	58.67	58.50	58.50
		k_{c1} [veh/km] FORMULA	28.75	30.50	30.74	30.61	30.95
		Q [veh/h] FORMULA	1983.5	1860.8	1803.6	1790.6	1810.4
		k_{c2} [veh/km] FORMULA	67.77	67.09	71.17	67.36	65.90
		ω [km/h] FORMULA	-15.00	-14.00	-14.00	-13.50	-13.50
		k_j [veh/km] FIXED	200	200	200	200	200
	2 - SL	V_f [km/h] FORMULA	68.00	52.25	52.50	53.00	53.50
		k_{c1} [veh/km] FORMULA	26.46	35.65	36.76	38.04	37.07
		Q [veh/h] FORMULA	1799.5	1862.7	1929.9	2016.0	1983.0
		k_{c2} [veh/km] FORMULA	71.46	67.64	63.37	60.97	63.24
		ω [km/h] FORMULA	-14.00	-14.07	-14.13	-14.50	-14.50
		k_j [veh/km] FIXED	200	200	200	200	200
SqE	1 - ML	V_f [km/h] VARIABLE	67.69	61.98	58.12	57.94	58.43
		k_{c1} [veh/km] FORMULA	29.30	30.02	31.03	30.90	30.99
		Q [veh/h] FORMULA	1983.5	1860.8	1803.6	1790.6	1810.4
		k_{c2} [veh/km] FORMULA	46.05	30.02	36.97	31.66	30.99
		ω [km/h] VARIABLE	-12.88	-10.95	-11.06	-10.64	-10.71
		k_j [veh/km] FIXED	200	200	200	200	200
	2 - SL	V_f [km/h] VARIABLE	66.60	51.66	53.89	56.76	56.14
		k_{c1} [veh/km] FORMULA	27.02	36.06	35.81	35.52	35.33
		Q [veh/h] FORMULA	1799.5	1862.7	1929.9	2016.0	1983.0
		k_{c2} [veh/km] FORMULA	45.28	37.81	35.81	35.52	35.33
		ω [km/h] VARIABLE	-11.63	-11.48	-11.75	-12.26	-12.04
		k_j [veh/km] FIXED	200	200	200	200	200
CSqE	1 - ML	V_f [km/h] VARIABLE	67.83	60.39	58.18	57.99	58.07
		k_{c1} [veh/km] FORMULA	28.47	29.97	29.76	29.35	29.37
		Q [veh/h] VARIABLE	1931.2	1809.6	1731.1	1701.7	1705.5
		k_{c2} [veh/km] FORMULA	50.71	30.27	44.37	40.90	40.51
		ω [km/h] VARIABLE	-12.94	-10.66	-11.12	-10.70	-10.69
		k_j [veh/km] FIXED	200	200	200	200	200
	2 - SL	V_f [km/h] VARIABLE	66.80	51.71	52.19	52.65	53.23
		k_{c1} [veh/km] FORMULA	26.11	34.36	35.81	35.52	35.33
		Q [veh/h] VARIABLE	1743.8	1776.8	1868.8	1870.5	1880.7
		k_{c2} [veh/km] FORMULA	50.89	46.10	35.81	35.52	35.33
		ω [km/h] VARIABLE	-11.69	-11.55	-11.38	-11.37	-11.42
		k_j [veh/km] FIXED	200	200	200	200	200

** FORMULA: the parameter was calculated with the formulas described in Section 2.7. VARIABLE: the parameter is an optimization variable. FIXED: the parameter is set and does not change.*

Table 9: Sum of the squared errors with fundamental diagram based [FD], squared error based [SqE], and constrained squared error based [CSqE] methods for the Measured Leader (ML) and Simulated Leader (SL) approaches

Indicator	Optimization method	Calibration Approach	SCENARIOS				
			A - 5.00 m	**B** - 2.50 m	**C** - 1.00 m	**D** - 0.10 m	**E** - 0.01 m
δ^2_{flow} $\left[\frac{veh}{h}\right]^2$	**FD**	1 - ML	19,111,618	54,692,630	35,916,542	37,654,133	39,291,455
		2 - SL	22,305,828	29,743,837	39,108,259	55,553,211	50,810,698
	SqE	1 - ML	1,328,577	1,918,611	1,251,285	1,179,218	1,218,025
		2 - SL	1,491,454	1,040,228	2,091,634	7,979,924	4,381,458
	CSqE	1 - ML	1,161,989	1,136,268	1,127,559	1,121,668	1,122,096
		2 - SL	1,284,608	956,262	845,442	919,216	894,184

Table 10: RMSE of the flow-density with fundamental diagram based [FD], squared error based [SqE], and constrained squared error based [CSqE] methods for the Measured Leader (ML) and Simulated Leader (SL) approaches

Indicator	Optimization method	Calibration Approach	SCENARIOS				
			A - 5.00 m	**B** - 2.50 m	**C** - 1.00 m	**D** - 0.10 m	**E** - 0.01 m
$RMSE_{flow}$ $\left[\frac{veh}{h}\right]$	**FD**	1 - ML	138.24	233.86	189.52	194.05	198.22
		2 - SL	149.35	172.46	197.76	235.70	225.41
	SqE	1 - ML	36.45	43.80	35.37	34.34	34.90
		2 - SL	38.62	32.25	45.73	89.33	66.19
	CSqE	1 - ML	**34.09**	33.71	33.58	33.49	33.50
		2 - SL	35.84	**30.92**	**29.08**	**30.32**	**29.90**

The results for the FD method show a higher free flow speed obtained in scenarios 1-A and 1-B, and the same stable results for scenarios 2-B to 2-E in terms of their free flow speed and shock-wave speed. The outflow capacity varies around 10% across the different scenarios, between 1790 and 2016 vehicles per hour.

The results for the CSqE method show the higher free flow speed obtained in scenarios 1-A and 1-B, and the same stable results for scenarios 2-B to 2-E in terms of their free flow speed and shock-wave speed. These results also provide the lowest RMSE around 30 [veh/h]. The free flow speed is lower in the scenarios of the simulated leader compared to the equivalent ones in the measured leader. The outflow capacity has a lower variation between the scenarios of the simulated leader, ranging between 1744 [veh/h] and 1881 [veh/h].

3.2.1 Fundamental diagrams of Fundamental Diagram based [FD] method

In the resulting fundamental diagrams, the difference of the flow between the macroscopic model and the microscopic model are concentrated in the congested section. This difference (plotted in grey on the secondary axis) is caused between the linear trend of the macroscopic model and a curved trajectory of the microscopic model, with a peak value at k_{c2}.

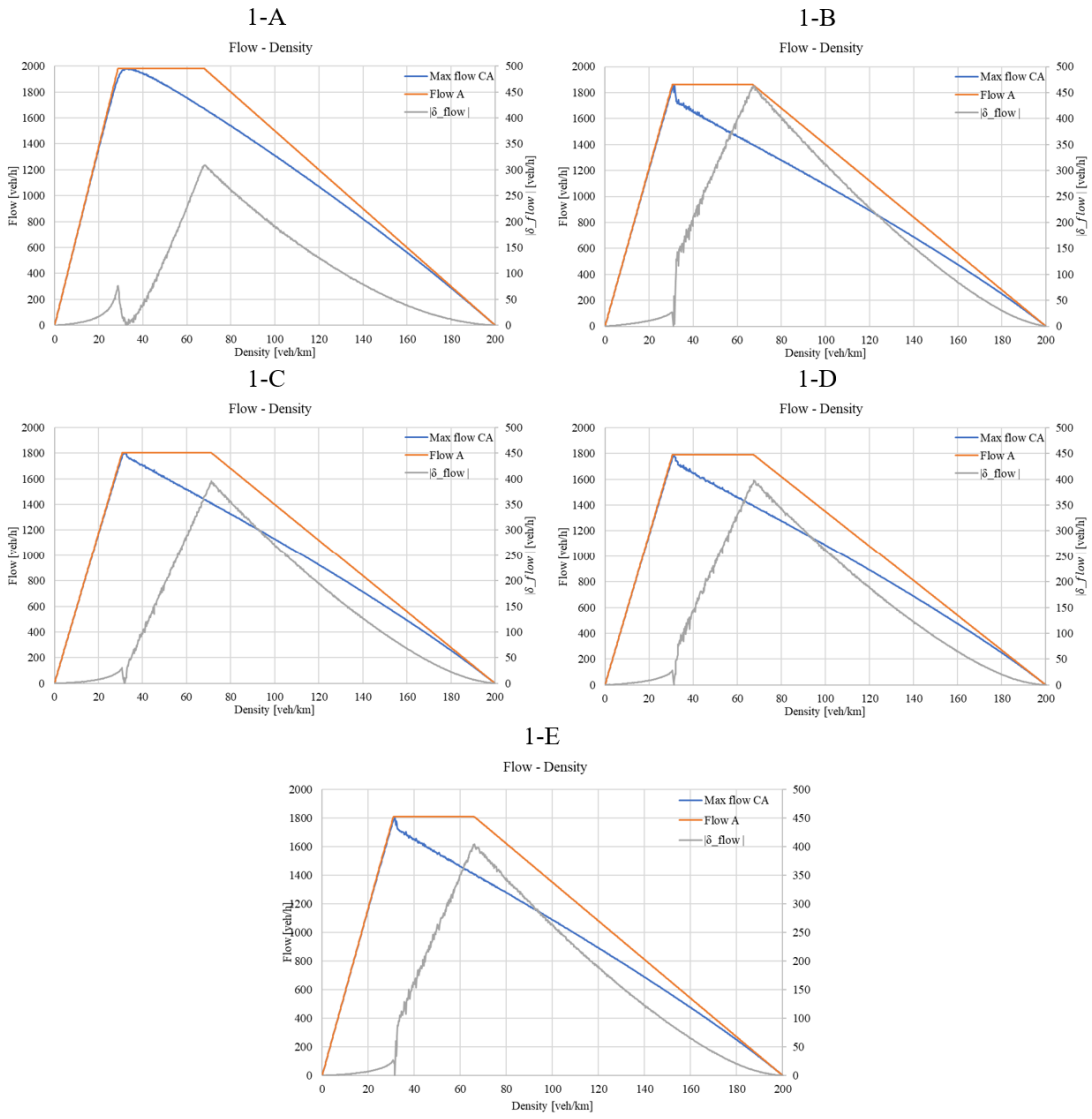

Figure 10 Flow – density diagrams of the macroscopic model for the Fundamental Diagram based [FD] method and Measured Leader approach

For the simulated leader approach, the abrupt transitions of scenarios 2-C to 2-E increases greatly the difference between the fundamental diagrams. In all cases, the parameters yield a trapezoidal fundamental diagram of the macroscopic model.

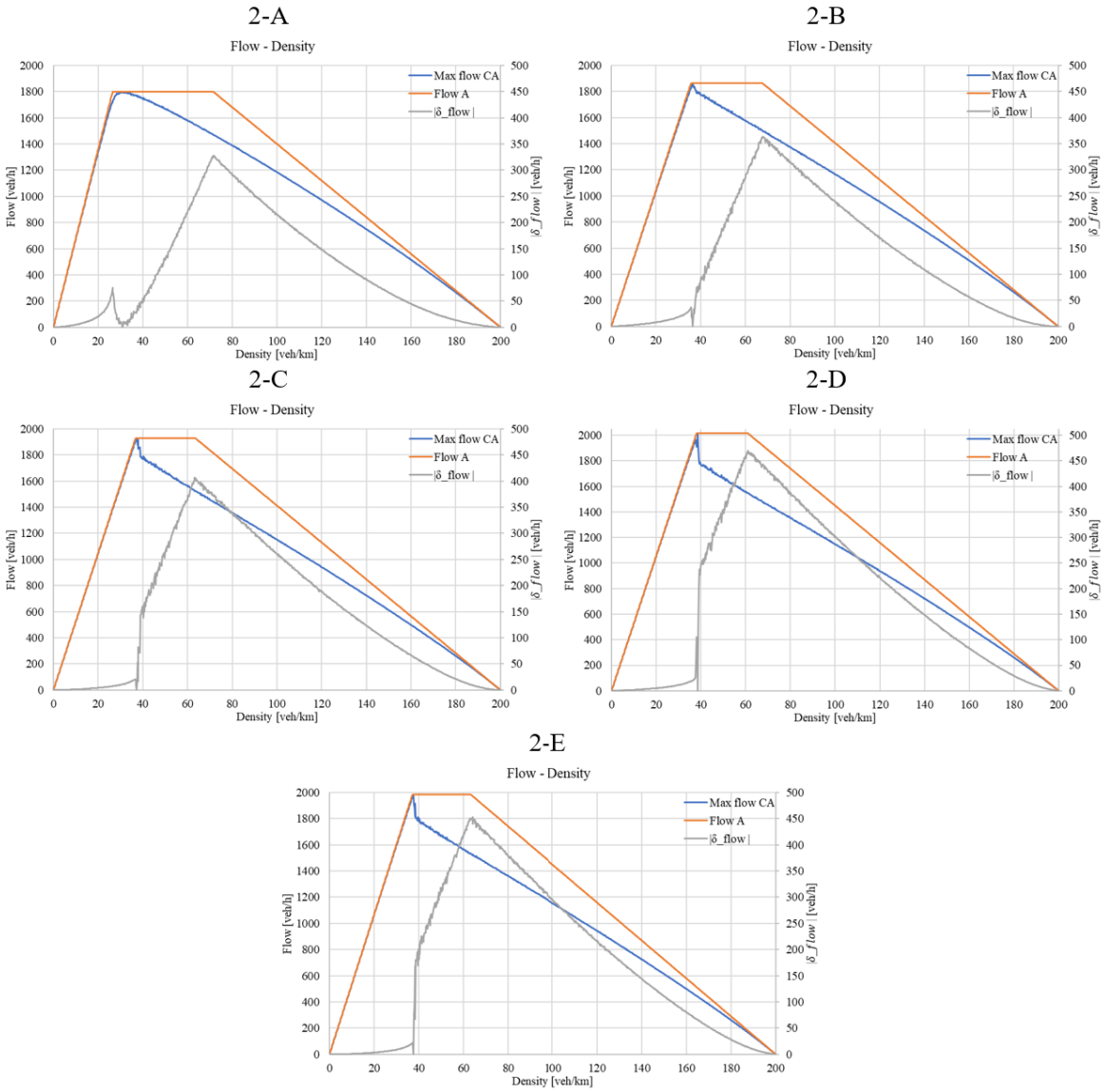

Figure 11 Flow - density diagrams of the macroscopic model for Fundamental Diagram based [FD] method and Simulated Leader approach

3.2.2 Fundamental diagrams of Squared Error based [SqE]Method

The resulting fundamental diagrams are closer to the microscopic model, giving lower errors than FD method. By imposing the condition ($k_{c1} \leq k_{c2}$) on the optimization procedure, the obtained free flow speed of scenarios 2-C to 2-E are higher than in the FD method. The fundamental diagram has a triangular shape, or almost, for scenarios B-E in both approaches. Only scenarios 1-A and 2-A with their smooth transition between congested and uncongested produce a trapezoidal shape.

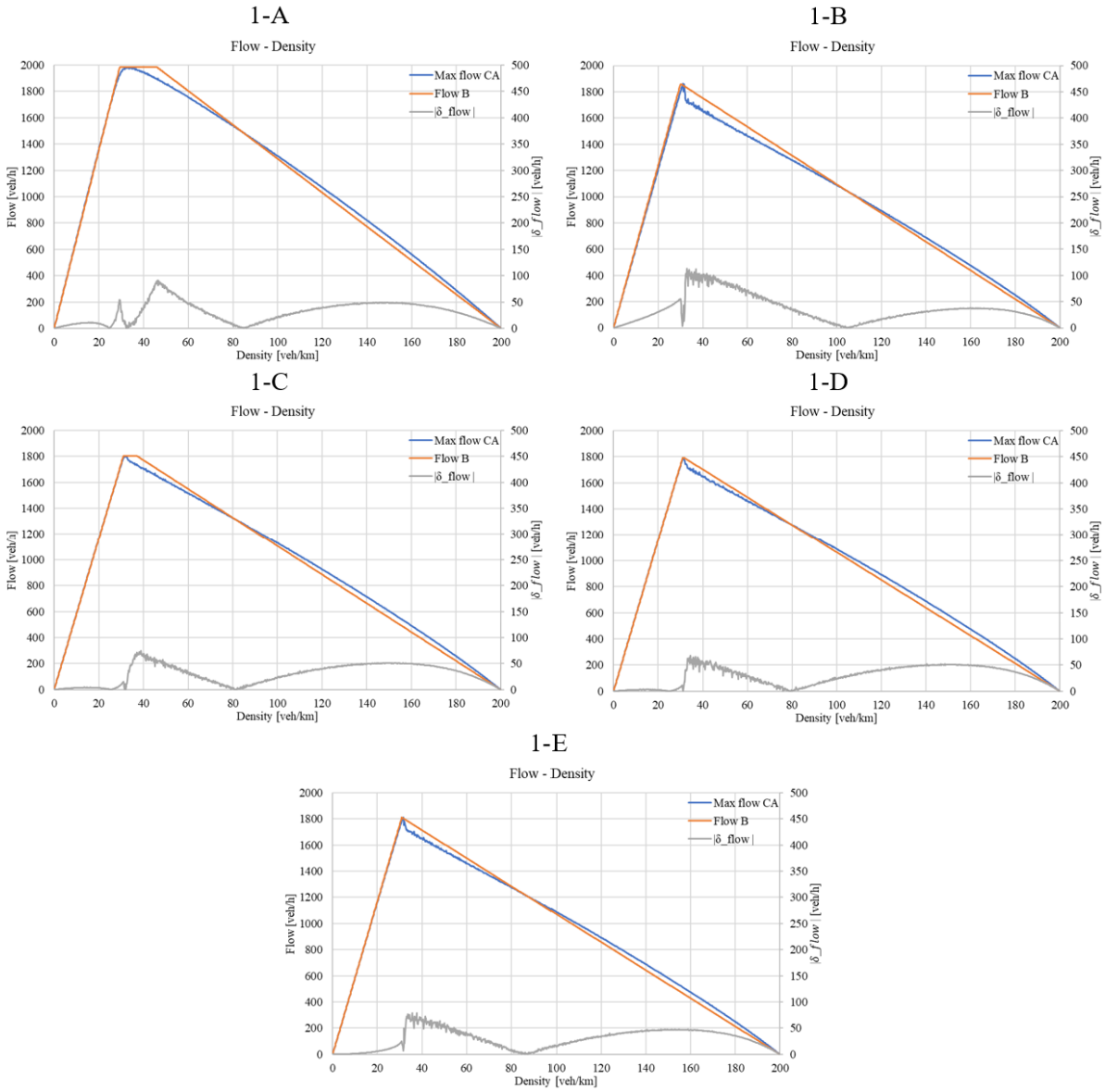

Figure 12 Flow - density diagrams of the macroscopic model for the squared error based [SqE] method and Measured Leader approach

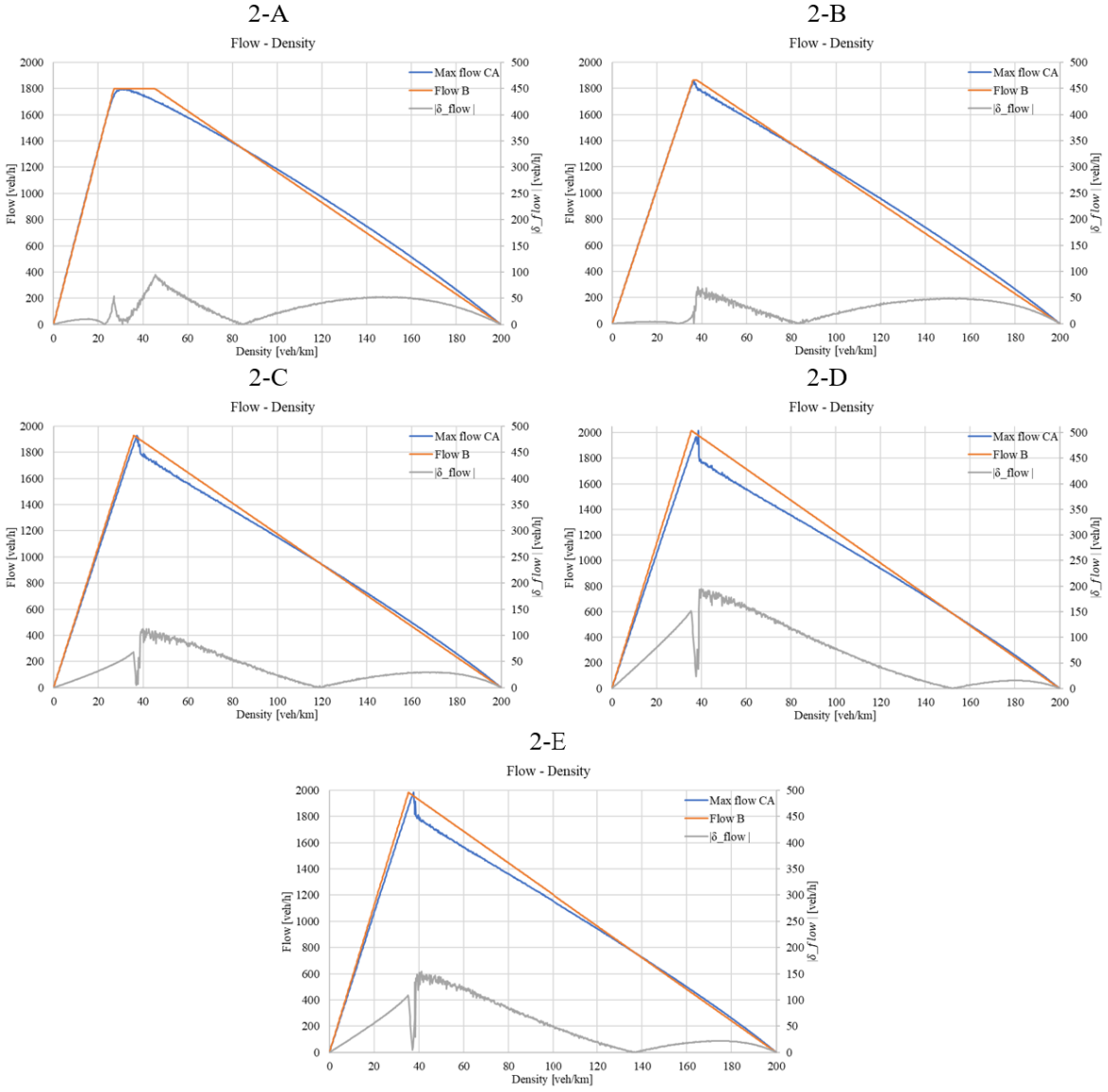

Figure 13 Flow - density diagrams of the macroscopic model for the squared error based [SqE] method and Simulated Leader approach

3.2.3 Fundamental diagrams of Constrained Squared Error [CSqE] method

The resulting fundamental diagrams are closer to the microscopic model, giving lower errors than the FD method. Scenarios 1-A and 2-A with their smooth transition between congested and uncongested produce a trapezoidal shape. The abrupt change between the congested and uncongested sections of scenarios 2-C to 2-E are limited with a triangular diagram on the macroscopic model that has a close free flow speed to the fundamental diagram of the microscopic model.

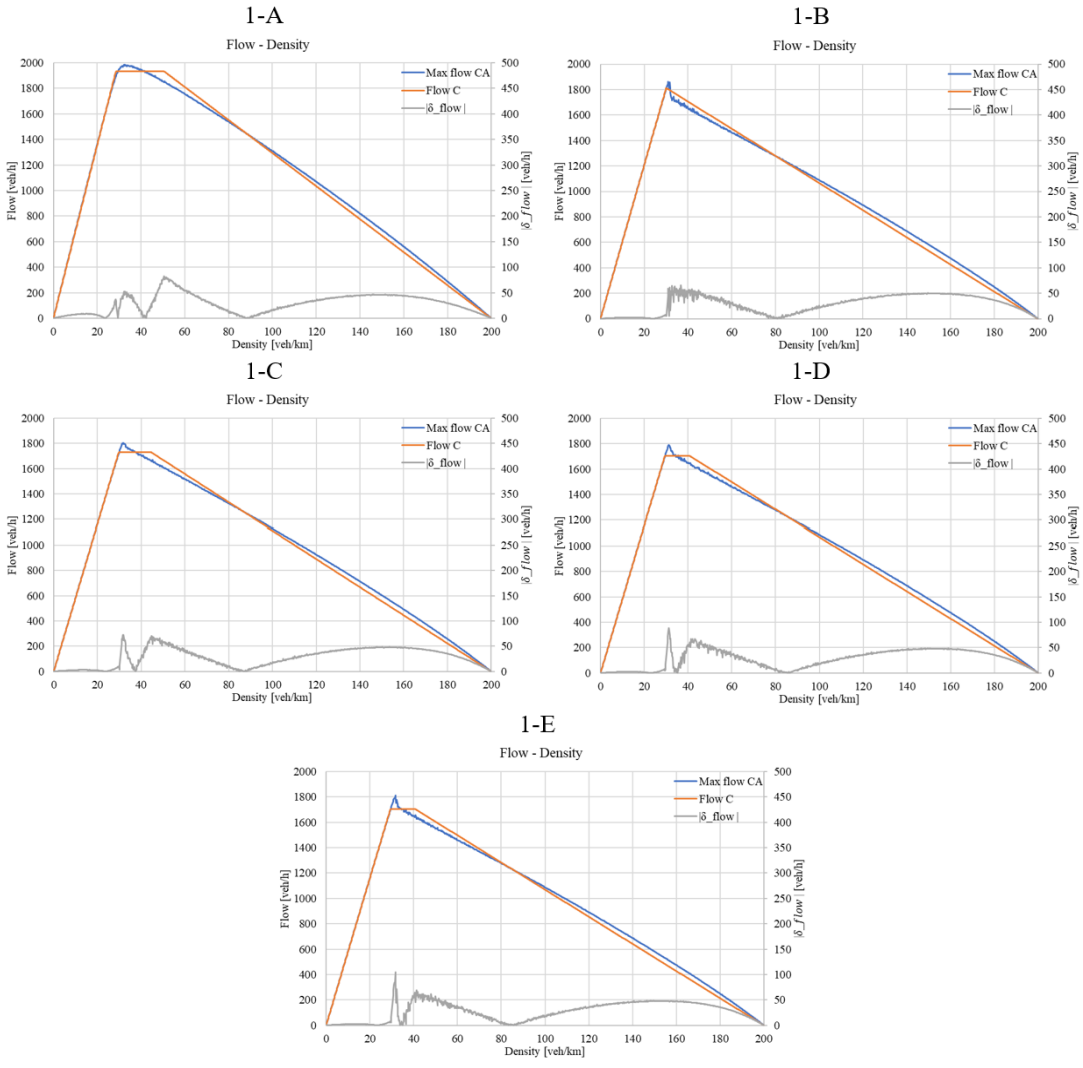

Figure 14 Flow - density diagrams of the macroscopic model for the constrained squared error based [CSqE] method and Measured Leader approach

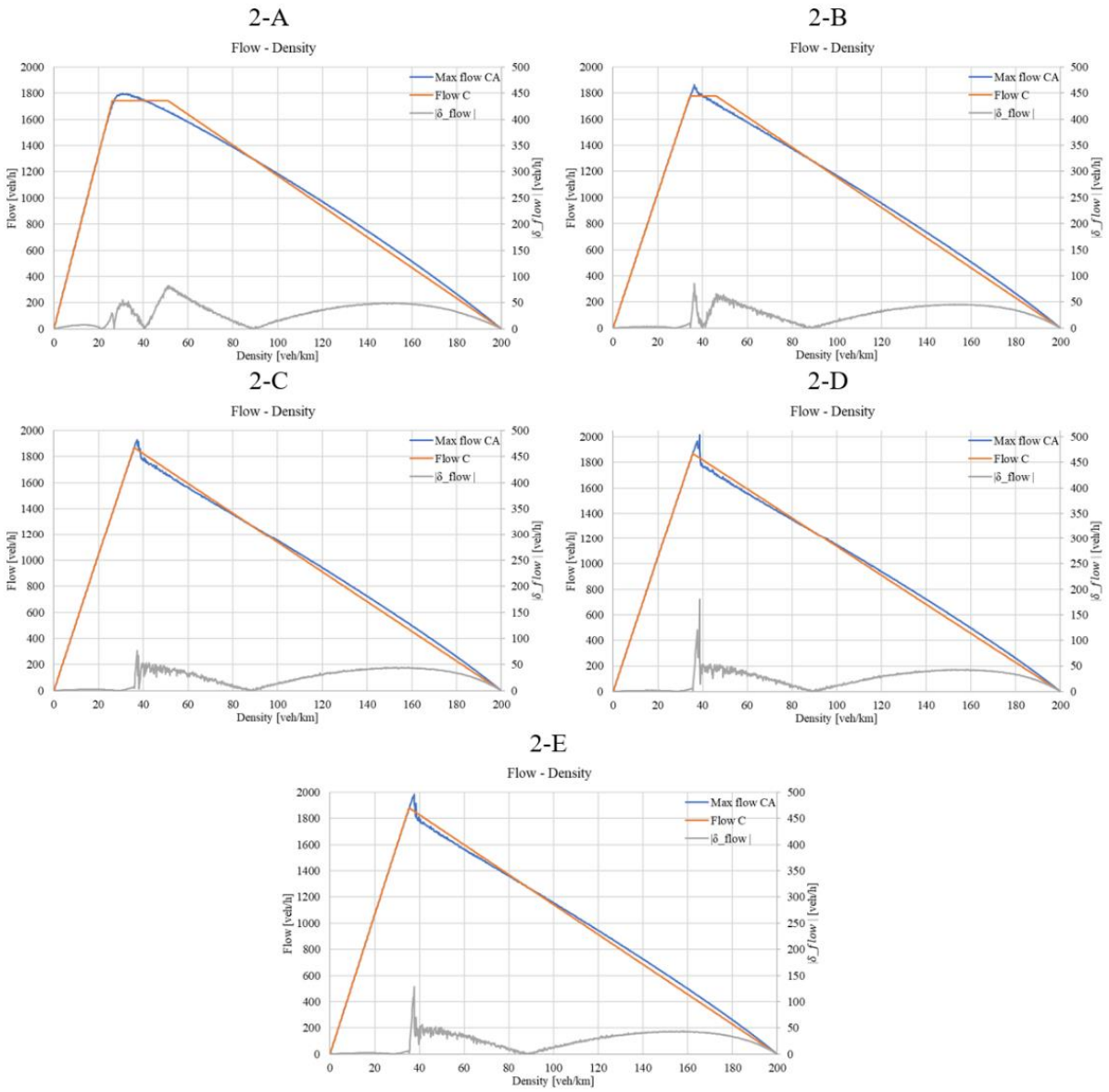

Figure 15 Flow - density diagrams of the macroscopic model for the constrained squared error based [CSqE] method and Simulated Leader approach

3.3 DISCUSSION

Analysing the results of the microscopic calibration listed in Table 3 and Table 4, it becomes apparent that the calibrated parameters obtained using the simulated leader approach (Table 4) exhibit greater regularity across various cell lengths (Scenarios 2B to 2E), particularly concerning the maximum speed and dawdling probability. This regularity is also reflected in the RMSE values.

A significant disparity in the overall objective function values (minimum mean RMSE) is observed between the measured leader (approximately 9 in the last row of Table 3) and the simulated leader approaches (around 290 for Table 4). The presence of a "measured" leader imposes a barrier influencing the behaviour of the modelled "follower vehicle", resulting in lower errors in its position and better depiction of a "following" behaviour. Conversely, in the simulated leader approach, the parameters obtained provide a better representation of the dynamics of the system, as the modelled vehicles have no external barrier or limitations influencing their behaviour on the circular road except for their interactions with each other.

In the cross analysis of Table 5, Table 6 and Table 7, applying the parameters from result 2A (simulated leader with a 5m cell length) to approach 1A (measured leader with a 5m cell length) yields the smallest difference compared to using calibrated parameters for approach 1A (-1.6%). Conversely, applying calibrated parameters from result 1A to approach 2A results in a substantial difference of +424.2% compared to the result obtained with the calibrated parameters for approach 2A. However, Result 2A also exhibits the highest RMSE among all simulated leader scenarios (106.66 versus less than 75). A smaller cell length provides a more accurate depiction of the interaction between vehicles, as evidenced by the decreasing RMSE from Scenarios 2B to 2E of Table 5, Table 6 and Table 7, when applied to the measured leader approach (18.47 for 2B down

to 10.54 for 2E). In contrast, the RMSE remains relatively constant in the simulated leader approach (between 71.11 and 74.46).

In the hybrid H-CA&CTM, each link integrates a microscopic CA model near the nodes and a macroscopic CTM along the link. Consequently, the CTM is bounded by the CA model both upstream and downstream. The CTM must be capable of receiving incoming flow from the CA in the first transition, and sending it back to the CA in the second transition, if there is no queue in the downstream CA. If the outflow capacity of the CTM is insufficient to handle the incoming flow from the CA, the first transition would be unable to cope with it, leading to a queue forming on the initial section of the link modelled by the microscopic CA. For this reason, the CTM should have a maximum outflow parameter close to the maximum flow of the CA model.

The constrained [CSqE] optimization method of the macroscopic calibrations showed the lowest sum of squared errors between the two fundamental diagrams (Table 9), with an uncongested part that is almost coincident, and a congested part in which the curved CA diagram is compensated with the linear approach of the CTM diagram (Figure 14 and Figure 15). Within the [CSqE] optimization method of the macroscopic calibration, result 2-C has the lowest $RMSE_{flow}$ indicator (29.08 veh/h in Table 10), since the steep transition between uncongested and congested parts of the CA fundamental diagram is more contained than in results 2-D and 2-E (Figure 15).

In the cross-analysis, the Simulated Leader approach 2 showed lower errors in the leader-follower interaction analysis (approach 2 applied on 1) compared to the Measured Leader approach 1 in the global behaviour analysis (approach 1 applied on 2). For an extensive-network study, the results of the simulated leader calibration approach should be considered, as it provides a better description of the overall behaviour of the system. For this purpose, results 2-B and 2-C with cell lengths of 2.5 metres and 1 metre may be the

best suited, maintaining a realistic acceleration coefficient. However, while result 2-A provides higher (and less real) accelerations and random decelerations of 5 m/s^2, the overall analysis considering its RMSE is aligned with those of 2-B and 2-C.

It is worth recalling that the experimental runs used for these calibrations were on a closed circular road with 37 to 49 vehicles per kilometre, corresponding to the slightly congested section of the resulting fundamental diagrams, close to their critical density. For urban or semi-urban applications, these results may be applicable. However, for an extra-urban analysis, the free flow speed may be increased, as the obtained 72 and 54 km/h of results 2-A to 2-C of Table 4 could be unsuitable in this context (20 m/s and 15 m/s).

It is also worth noting the effect of the dawdling probability on the overall free flow speed of the CA model. Considering that the maximum speed in the CA is 72 and 54 km/h for the results of the simulated leader 2-A and 2-B/C respectively, the free flow speed in the macroscopic fundamental diagrams is close to 67 and 52 km/h for the same scenarios using the constrained squared error based [CSqE] optimization method (Table 8).

4 CONCLUSIONS

The impact of cooperative connected and automated mobility strategies can be referred to local contexts and other more extensive contexts on a very large-scale network application. Regarding traffic flow modelling, specific traffic flow models are required to support suitable representation of vehicle (driver) behaviour, using the information provided by connected vehicles. Microscopic models are typically employed to address this issue as they can handle each vehicle individually. However, such models are highly detailed, require several parameters to be set, and are computationally demanding. Consequently, an alternative modelling approach based on a hybrid model can be adopted to overcome these challenges. In this context, the hybrid multi-scale approach (Leclercq, 2004) emerges as a viable solution. A multi-scale framework can leverage microscopic,

disaggregated modelling in areas where traffic control strategies are implemented, while employing macroscopic modelling in other areas indirectly influenced by the controlled infrastructure. In particular, the proposed hybrid model can be utilized to implement traffic management strategies in the presence of both human-driven and connected automated vehicles, thus enabling cooperative optimisation (see Di Pace et al., 2022).

This paper focused on a model already developed in the literature, the H – CA&CTM (Hybrid Cellular Automata Cell Transmission Model, Storani et al., 2022) which combines the cellular automata model (CA; Nagel and Schreckenberg, 1992) with the cell transmission model (CTM; Daganzo, 1994). The aim of the paper aims is threefold:

1. Investigate the calibration of the CA model concerning various cell lengths through two distinct approaches: simulating all vehicles together in a closed ring layout and simulating each vehicle using data obtained from its respective follower.
2. Explore different methods for the calibration of the macroscopic CTM with respect to the CA model.
3. Utilize vehicle trajectory data collected from a car-following field experiment on a circular road track for the calibration procedure. This makes possible a comprehensive comparison of methods.

In more detail, to calibrate the CA model two approaches were considered: i) Measured Leader – Simulated Follower interaction approach; ii) Simulated Leader - Simulated Follower interaction approach. To derive the fundamental diagram of the microscopic model, a circular road was simulated.

Results obtained with the Simulated Leader approach, particularly focusing on scenarios with cell lengths of 2.5 meters and 1 meter, show a regular trend. Indeed, these results exhibit greater regularity across various cell lengths concerning maximum speed and dawdling probability, indicating a more accurate depiction of vehicle interactions. Additionally, these specifications maintain a realistic acceleration coefficient, which is crucial for capturing real-world dynamics.

Concerning the CTM calibration three approaches were evaluated: a fundamental diagram based [FD], a squared error based [SqE], and a constrained squared error based [CSqE] method. In particular, in the [FD] method the free flow speed, the shockwave speed and the maximum outflow capacity are all obtained directly from the results of the fundamental diagrams of the CA; in the [SqE] method, the maximum outflow capacity is obtained directly from the results of the fundamental diagrams of the CA whilst the free flow speed and the shockwave speed are obtained by minimizing the sum of the squared error; for the [CSqE] method, the free flow speed, the shockwave speed and the maximum outflow capacity are all obtained by minimizing the sum of the squared error, with the same optimization objective and flow equation of the [SqE] method.

In the H-CA&CTM model, the CTM model is bounded by the CA model both upstream and downstream. Therefore, the CTM should have a maximum outflow parameter close to the maximum flow of the CA model. The Constrained Squared Error [CSqE] method for the macroscopic calibrations showed promising results, demonstrating the lowest sum of squared errors between fundamental diagrams. These results also provide the lowest RMSE around 30 [veh/h] suggesting a more contained transition between uncongested and congested parts of the CA fundamental diagram. The free flow speed is lower in the scenarios of the simulated leader compared to the equivalent ones in the measured leader.

The major findings of the paper are: 1) the calibrated parameters obtained using the simulated leader approach display greater regularity across different cell lengths; 2) the Constrained Squared Error [CsqE] method for macroscopic calibrations yielded promising results, showcasing the lowest sum of squared errors between fundamental diagrams.

Considering the applicability of the model to various contexts, it is essential to acknowledge the experimental conditions under which the calibrations were conducted. The circular road track used for data collection represented a slightly congested section, close to its critical density. Thus, for urban or semi-urban applications, the specified model parameters may be applicable, but adjustments may be necessary for extra-urban analysis, particularly in increasing the free flow speed.

In future works, the improved H-CA&CTM, capable of analysing mixed traffic flow conditions with both human-driven and connected automated vehicles, will be specified and calibrated. Additionally, the model will be applied to a real case study. Ultimately, the model will be integrated with lane-changing rules.

ACKNOWLEDGMENTS

This study was carried out within the MOST – Sustainable Mobility National Research Centre and received funding from the European Union Next-GenerationEU (PIANO NAZIONALE DI RIPRESA E RESILIENZA (PNRR) – MISSIONE 4 COMPONENTE 2, INVESTIMENTO 1.4 – D.D. 1033 17/06/2022, CN00000023). This manuscript

reflects only the authors' views and opinions, neither the European Union nor the European Commission can be considered responsible for them.

This research was partially funded by the University of Salerno, under local grants no. ORSA214124-2021, no. ORSA223793– 2022 and no.ORSA238719 -2023

It was also partially funded by the project DIGIT-CCAM "Progetti di Rilevante Interesse Nazionale" (PRIN 2020 -MUR), and I CAN BE "Progetti di Rilevante Interesse Nazionale" (PRIN 2022 -MUR).

Authors wish to thank anonymous reviewers for their helpful comments.

REFERENCES

Cascetta E. (2009). Transportation Systems Analysis: Models and Applications. Springer. 448–477

Chen, W. Y., Huang, D. W., Huang, W. N., & Hwang, W. L. (2004). Traffic flow on a 3-lane highway. International Journal of Modern Physics B, 18(31n32), 4161-4171.

Chowdhury, D., Wolf, D. E., & Schreckenberg, M. (1997). Particle hopping models for two-lane traffic with two kinds of vehicles: Effects of lane-changing rules. Physica A: Statistical mechanics and its applications, 235(3-4), 417-439.

Daganzo, C. F. (1994). The cell transmission model: A dynamic representation of highway traffic consistent with the hydrodynamic theory. *Transportation research part B: methodological*, *28*(4), 269-287.

Degrande, T., Vannieuwenborg, F., Verbrugge, S., & Colle, D. (2023). Deployment of Cooperative Intelligent Transport System infrastructure along highways: A bottom-up societal benefit analysis for Flanders. *Transport policy*, *134*, 94-105.

Di Pace, R, Storani F., de Luca, S. (2023) Technical Report - Deliverable 3.4.2 Study area identification; traffic zones identification of the basic network *Research Project: MOST – Sustainable Mobility National Research Center – Spoke 7, October 2023*

Di Pace, R., Fiori, C., Storani, F., de Luca, S., Liberto, C., & Valenti, G. (2022). Unified network tRaffic management frAmework for fully conNected and electric vehicles energy cOnsumption optimization (URANO). *Transportation Research Part C: Emerging Technologies, 144, 103860.*

Jia, B., Jiang, R., & Wu, Q. S. (2004). A realistic two-lane cellular automaton model for traffic flow. *International Journal of Modern Physics C, 15(03), 381-392.*

Jia, B., Jiang, R., Wu, Q. S., & Hu, M. B. (2005). Honk effect in the two-lane cellular automaton model for traffic flow. *Physica A: statistical mechanics and its applications, 348, 544-552.*

Khan, M. J., Khan, M. A., Ullah, O., Malik, S., Iqbal, F., El-Sayed, H., & Turaev, S. (2023). Augmenting CCAM Infrastructure for Creating Smart Roads and Enabling Autonomous Driving. *Remote Sensing*, *15*(4), 922.

Knospe, W., Santen, L., Schadschneider, A., & Schreckenberg, M. (1999). Disorder effects in cellular automata for two-lane traffic. *Physica A: Statistical Mechanics and its Applications, 265(3-4), 614-633.*

Knospe, W., Santen, L., Schadschneider, A., & Schreckenberg, M. (2002). A realistic two-lane traffic model for highway traffic. *Journal of Physics A: Mathematical and General, 35(15), 3369.*

Kurata, S., & Nagatani, T. (2003). Spatio-temporal dynamics of jams in two-lane traffic flow with a blockage. *Physica A: Statistical Mechanics and its Applications, 318(3-4), 537-550.*

Laval, J. A., Toth, C. S., & Zhou, Y. (2014). A parsimonious model for the formation of oscillations in car-following models. Transportation Research Part B: Methodological, 70, 228-238.

Leclercq, L. (2007). Hybrid approaches to the solutions of the "Lighthill–Whitham–Richards" model. *Transportation Research Part B: Methodological*, *41*(7), 701-709.

Lee, S. E., Olsen, E. C., & Wierwille, W. W. (2004). A comprehensive examination of naturalistic lane-changes (No. FHWA-JPO-04-092). United States. Department of Transportation. National Highway Traffic Safety Administration.

Li, X. G., Jia, B., Gao, Z. Y., & Jiang, R. (2006). A realistic two-lane cellular automata traffic model considering aggressive lane-changing behavior of fast vehicle. *Physica A: Statistical Mechanics and its Applications, 367, 479-486.*

Lu, J., & Zhou, X. S. (2023). Virtual track networks: A hierarchical modelling framework and open-source tools for simplified and efficient connected and automated mobility (CAM) system design based on general modelling network specification (GMNS). *Transportation Research Part C: Emerging Technologies*, *153*, 104223.

Maerivoet, S., & De Moor, B. (2005). Cellular automata models of road traffic. *Physics reports, 419(1), 1-64.*

Nagai, R., Nagatani, T., & Taniguchi, N. (2005). Traffic states and jamming transitions induced by a bus in two-lane traffic flow. *Physica A: Statistical Mechanics and its Applications, 350(2-4), 548-562.*

Nagel, K., & Nelson, P. (2005). A critical comparison of the kinematic-wave model with observational data. In Transportation and Traffic Theory. Flow, Dynamics and Human Interaction. 16th International Symposium on Transportation and Traffic TheoryUniversity of Maryland, College Park.

Nagel, K., & Schreckenberg, M. (1992). A cellular automaton model for freeway traffic. *Journal de physique I*, *2*(12), 2221-2229.

Nagel, K., Wolf, D. E., Wagner, P., & Simon, P. (1998). Two-lane traffic rules for cellular automata: A systematic approach. *Physical Review E, 58(2), 1425.*

Rickert, M., Nagel, K., Schreckenberg, M., & Latour, A. (1996). Two lane traffic simulations using cellular automata. *Physica A: Statistical Mechanics and its Applications, 231(4), 534-550.*

Storani, F., Di Pace, R., & De Luca, S. (2022). A hybrid traffic flow model for traffic management with human-driven and connected vehicles. *Transportmetrica B: transport dynamics*, *10*(1), 1151-1183.

Tian, J., Li, G., Treiber, M., Jiang, R., Jia, N., & Ma, S. (2016). Cellular automaton model simulating spatiotemporal patterns, phase transitions and concave growth pattern of oscillations in traffic flow. *Transportation Research Part B: Methodological*, 93, 560-575.

Tian, J., Zhu, C., Chen, D., Jiang, R., Wang, G., & Gao, Z. (2021). Car following behavioral stochasticity analysis and modelling: Perspective from wave travel time. *Transportation Research Part B: Methodological*, 143, 160-176.

Tordeux, A., Roussignol, M., Lebacque, J. P., & Lassarre, S. (2014). A stochastic jump process applied to traffic flow modelling. *Transportmetrica A: Transport Science, 10(4), 350-375.*

Treiber, M., & Kesting, A. (2013). Traffic flow dynamics. *Traffic Flow Dynamics: Data, Models and Simulation, Springer-Verlag Berlin Heidelberg*, 983-1000.

Yang, H. F., Cai, J., Liu, C., Ke, R., & Wang, Y. (2023). Cooperative multi-camera vehicle tracking and traffic surveillance with edge artificial intelligence and representation learning. *Transportation research part C: emerging technologies*, *148*, 103982.

Zhao, W., Liu, R., & Ngoduy, D. (2021). A bilevel programming model for autonomous intersection control and trajectory planning. *Transportmetrica A: transport science*, 17(1), 34-58.

Zheng, S. T., Jiang, R., Tian, J. F., Zhang, H. M., Li, Z. H., Gao, L. D., & Jia, B. (2021). Experimental study on properties of lightly congested flow. *Transportation Research Part B: Methodological*, 149, 1-19.

Zhou, S., Zheng, S., Treiber, M., Tian, J., & Jiang, R. (2023). On the calibration of stochastic car following models. *arXiv preprint arXiv:2302.04648*.